Stony Brook University

Melting Characteristic of Polymer Thin and Ultra-Thin Films

A Thesis Presented

By

Wei Liu

to

The Graduate School

in Partial Fulfillment of the

Requirements

for the Degree of

Master of Science

in

Materials Science and Engineering

Stony Brook University

May 2008

Stony Brook University

The Graduate School

Wei Liu

We, the thesis committee for the above candidate for the
Master of Science degree, hereby recommend
acceptance of this thesis

Jonathan C. Sokolov, Professor, Thesis Advisor
Department of Materials Science and Engineering

Miriam Rafailovich, Professor
Department of Materials Science and Engineering

Tadanori Koga, Assistant Professor
Department of Materials Science and Engineering

This thesis is accepted by the Graduate School

Lawrence Martin
Dean of the Graduate School

Abstract of the Thesis

Melting Characteristic of Polymer Thin and Ultra-Thin Films

by

Wei Liu

Master of Science

In

Materials Science and Engineering

Stony Brook University

2008

The research is mainly cast on the relationship between the melting temperature and film thickness with thin (100-300 nm) and ultra-thin (<100 nm) films of two semi-crystalline polymers, poly ethylene vinyl acetate (EVA770) and linear low-density polyethylene (LLDPE) spun casting on the silicon wafers by Atomic Force Microscopy (AFM) and self-designed Optical Test M`thod (OTM). The images of EVA770 and LLDPE samples are measured by Scanning Probe Microscope (SPM). The melting temperature of bulk films is also measured by Differential Scanning Calorimetry (DSC).

Experimental results indicate that between a given zone of polymer film thickness, the melting temperature increases largely with the thickness, above or below some certain film thickness, the melting temperature will show little variation. The maximum melting temperature gap between the thick (above 800 Å) and thin (below 200 Å) of EVA770 film is 21.5K by AFM and 23K by OTM, while the maximum melting temperature gap of LLPDE film is 25K by AFM, and 22K by OTM. This melting characteristic in OTM method is explained with Jones Calculus and Fresnel Equations.

Table of Contents

List of Figures

List of Tables

Acknowledgement

First of all, I want to express my sincere gratitude to professor Jonathan Sokolov and professor Miriam Rafailovich, for their supervision and unselfish help during my research experience in Garcia Center for Polymer, this period is so short and past so fast, much knowledge has been poured into my mind, including their great spirit to science and always be helpful to the students.

Also I would like thank professor Dilip Gersappe, from whom I got instructions and much help during my study.

I would like thank professor Tadanori Koga for his kind help and good suggestion.

I would like to express my appreciation to Dr. Shouren Ge, Dr. Song Li, Dr. Yantian Wang, Dr. Chunhua Li, who gave me a lot of help during my experiment.

I would thank all the other partners in Garcia Center, whom I was happy to work with and supported each other.

1. Introduction

1.1 Introduction of Thin and Ultra- thin Polymer Film

1.1.1 Thin and Ultra-thin Polymer film

Interests increase fast for the polymer thin film application in the industry in recent years, due to great necessary in such areas as electronics, optics, biomedicals etc, [1]. It has been reported that polymer film thickness, molecular weight, and cross-linking density can greatly affect the thermo-physical properties of polymer thin film, such as glass transition temperature, coefficient of thermal expansion and electro-optical properties [2]. Among these elements, the size dependence of the thermo-physical properties of thin (100-300 nm) and ultra-thin (<100 nm) polymer films is the subject of strong concern for experimental, technological and theoretical issue [3, 4].

One important advantage of thin and ultra-thin polymer film is that they are highly selective and highly sensitive and can be tailored with desired functions, bio-reactive properties and incorporated into electronics, optical and electrochemical devices. The typical examples are polymethyl methacrylate (PMMA) coatings for lithography of integrated circuits and micromechanical devices [5], the molecular dimensions of the polymer thin films make the development of sophisticated system possible.

In confined environment, the properties of thin and ultra-thin polymer film show quite different from those of bulk polymers, due to the interference of intrinsic length scales with the dimensions of the imposed geometry [6]. Further work on this issue will be important perquisite to the use of nano-polymer materials.

1.1.2 Melting Behavior of Polymer Thin Film

Polymer materials are large molecules with intermolecular forces and tangled chains. They can be classified into three types, crystalline polymers, amorphous polymers and semi-crystalline polymers. Highly crystalline polymers (95-99%) are rigid, high melting point and less affected by solvent penetration, crystalline polymer is now known

that may form lamellar (plate-like) crystals with a thickness of 10-20nm in which the parallel chains perpendicular to the face of the crystals.

Amorphous polymers are branches or irregular pendant groups which can not pack together regularly enough to form crystalline, amorphous regions of a polymer are made up of randomly coiled and entangled chains.

Semi-crystalline polymers have both crystalline and amorphous region, the crystalline portion is in the lamellar, the amorphous portion is outside the lamellae, the crystalline potion is small and connected to the amorphous regions by polymer chains [7, 8].

The softening, melting and flowing process of polymer depend on the polymer morphology (amorphous and crystalline of polymer), From Fig 1(1), we know that when a crystalline polymer is heated at a constant rate, the temperature increases at a constant rate, when the temperature reaches the melting temperature T_m (or T_f), there is sharp transition, the temperature hold steady until the polymer has completely melted into liquid, then the temperature will continue to increase.

The amorphous polymers lack sufficient regularity in packing of the chains compared to the crystalline polymer, below glass transition temperature T_g, amorphous polymers exist as hard, rigid and glassy matter, where motion is restricted to molecular motions. When the temperature is above T_g, segments (20-50 atoms) of the entangled chains can move, the polymer becomes soft and flexible, the substance becomes rubbery state, as showed in Fig 1(2).

Semi-crystalline polymers have both crystalline and amorphous regions, therefore, T_g and T_m exist together in semi-crystalline. Above the T_m, the crystalline section melts into liquid, below T_m, the crystalline becomes cold crystallization, T_g is always lower than T_m [9.10].

In recent years, some work has been done on the thickness-dependent T_g or T_m of polymer films [11, 12, 13, 14,]. It is reported that for those polymer films which have favorable interaction with the substrate, T_g (or T_m) increases with the thickness. If the polymers have no significant interaction with the substrate, T_g (or T_m) may either increase, decrease or remain the same [15]. For example, it was found that the melting

point of poly (ethylene-vinyl acetate) (EVA) thin films (below 30 nm) dropped 15K compared to the bulk polymer by Kim [16]. It is observed that a T_m large change of up to 38K for linear low-density polyethylene (LLDPE) when thickness under 150 nm [17].

On the other hand, some experiments indicated that T_m of PCL (poly (ε-caprolactone)) on quartz or hydrophobic silicon substrates, does not appear to vary with film thickness [18]. Also, C.C. White measured the T_g of five polystyrene films in the thickness range from 25nm to 200nm on quarts substrates, and found that T_g of the five ultra-thin films was similar to the bulk T_g with no dependence on the thickness [11].

In this paper, Differential Scanning Calorimetry (DSC) is used to measure the melting temperature of bulk polymer films, other techniques such as Atomic Force Microscope (AFM) and new- designed Optical Test Methods (OTM) are applied to measure the T_m for a series of thickness polymer films. Two kinds of widely-used polymers are studied, poly ethylene vinyl acetate (EVA770) and linear low-density polyethylene (LLDPE). EVA770 is the copolymer of ethylene vinyl and acetate. EVA 770 used is made by Dupont Packaging & Industrial Company, it is an EVA (ethylene vinyl acetate copolymer) plastic materials, includes 9.5% (by weight) ethylene vinyl, it can be used in a variety of applications involving molding, compounding, extrusion, adhesives, sealants and wax blends. The typical properties of Elvax 770 are in Table 1[19].

Physical	Nominal Values	Test Methods
Density	$0.93 g/cm^3$	ASTM D792 ISO1183
Melt Index(190^0C/2.16kg)	0.8g/10min	ASTM D1238 ISO1133
Thermal	Nominal Values	Test Methods
Melting Point (DSC)	96^0C	ASTM D3418 ISO3146
Vicat Softening Point(^{0}C)	80^0C	ASTM D1525 ISO306

Table 1 Typical Properties of EVA770

Linear low-density polyethylene (LLDPE) is a substantially linear polymer with numbers of short branches, commonly made by copolymerization of ethylene with longer-chain olefins. The typical properties of LLDPE are in Table 2.

Properties	Density	Hardness	Tensile strength	Melting Point
Values	$0.92g/cm^3$	D47	1700psi	118^0C

Table 2 Typical Properties of Linear Low-density Polyethylene (LLDPE)

Both EVA770 and linear LLDPE are semi-crystalline polymers.

1.2 Polarized Light and Birefringence

1.2.1 Polarization and Birefringence of Light

` Light can be described as an electromagnetic wave produced by vibrating electric charges. When a light wave is vibrating in more than one plane, it is said to be un-polarized. Polarization is a process by which un-polarized light waves are combined into vibration along one single plane. There are three typical polarizations, linear polarization, circular polarization, and elliptical polarization. For the light propagating along z axis, linear polarization can be oriented in any direction perpendicular to the propagation direction and can be described as a vector sum of E_x and E_y. If the light is composed of two plane waves of equal amplitude but differing in phase 90^0, then the light is said to be circularly polarized. Elliptically polarized light consists of two perpendicular waves of unequal amplitude which differ in phase by 90° [20, 21].

An optical device whose input is natural light and whose output is some form of polarized light is called a polarizer. The physical uses for polarizer are dichroism or selective absorption, scattering, reflection and birefringence or double refraction. There are many practical applications of polarizer, including polarized sunglasses, stress

analysis tests on plastics, production and viewing of 3-D films, electronics and photography [22].

Birefringence is a property of optical materials for which light polarized along the x axis experience a difference index of refraction, and therefore travels at a different speed than does light polarized along the y axis. Birefringence comes from the anisotropy of some crystals, including hexagonal, tetragonal, and trigonal, which have different indices of refraction within their structures, this may cause light entering the crystal to refract into two rays that travel at different speeds [23].

1.2.2 Introduction of Calculus for Polarization Light

Jones Calculus, Mueller Calculus, and Poincare Sphere are three useful methods that describe polarization light. Jones Calculus and Mueller Calculus are matrix methods, in which, the light beam is represented by a vector, the optical device encountered by the beam is represented by a matrix, and they are multiplied to yield another vector representing the light beam output. Poincare Sphere is a graphical representation polarized light methods, it is simpler than the other methods and often rapidly yields the polarization information. The Jones Calculus can only be applied to fully polarization light, the Mueller Calculus can be used to partially polarization light as well as fully polarization light, but in Jones Calculus, phase information is retained, while there is no phase form in Mueller Calculus. In this study, the Jones Calculus is used, for the polarized light tested is nearly fully polarization light [24, 25].

According to Jones Calculus methods [26], if the time-dependent term is omitted, polarization light propagation in z-direction can be represented by Jones Vector as follows,

$$J = \begin{vmatrix} A_x \ell^{i\Phi_x} \\ A_y \ell^{i\Phi_y} \end{vmatrix} \quad (1.1)$$

Here A_x and A_y are the magnitudes of the electric field along X and Y axis, $Ø_x$ and $Ø_y$ are x-axis and y-axis phase terms.

The Jones vector for horizontally polarized light is,

$$J = \begin{vmatrix} A_x \ell^{i\vartheta_x} \\ 0 \end{vmatrix} \quad (1.2)$$

The Jones vector for vertically polarized light is,

$$J = \begin{vmatrix} 0 \\ A_y \ell^{i\vartheta_y} \end{vmatrix} \quad (1.3)$$

The Mueller Matrices for a linear polarizer is given as follows, while θ is the angle that the polarizer oriented from x-axis.

$$M(\theta) = \begin{vmatrix} \cos^2\theta & \sin\theta\cos\theta \\ \sin\theta\cos\theta & \sin^2\theta \end{vmatrix} \quad (1.4)$$

The Mueller Matrices for a linear retarder with azimuth ρ and retardation δ is given as,

$$M(\theta) = \begin{vmatrix} \cos^2\rho e^{i\delta/2} + \sin^2\rho e^{-i\delta/2} & 2i\sin\rho\cos\rho\sin(\delta/2) \\ 2i\sin\rho\cos\rho\sin(\delta/2) & \cos^2\rho e^{-i\delta/2} + \sin^2\rho e^{i\delta/2} \end{vmatrix} \quad (1.5)$$

The output effect is the result of light with the optical components. As the follows,

$$[Output] = [Mueller \quad Matrices][Input \quad Light] \quad (1.6)$$

$$\begin{vmatrix} E_x^{'} \\ E_y^{'} \end{vmatrix} = \begin{vmatrix} m_{11} & m_{12} \\ m_{21} & m_{22} \end{vmatrix} \begin{vmatrix} E_x \\ E_y \end{vmatrix} \quad (1.7)$$

$$E_x^{'} = m_{11}E_x + m_{12}E_y$$
$$E_y^{'} = m_{21}E_x + m_{22}E_y \quad (1.8)$$

E_x and E_y are Jones vector elements of the initial light beam, $E_x^{'}$ and $E_y^{'}$ are the Jones vector elements of the beam after it comes from the optical devices, and m_{ij} are coefficients determined by the optical properties of the devices encountered.

1.3 Reflection of Polarization Light

When a monochromatic light is incident on a dielectric material, the portion that is reflected or transmitted will depend on the polarization of the light, the angle of the incident, and the refractive indices of the two media [27]. The refracted light is described by the Snell's law as [28],

$$\theta_\gamma = \sin^{-1}\left(\frac{\sin\theta_i}{n}\right) \quad (1.9)$$

Where θ_i is the incident angle, θ_r is the refracted light angle, n is the index of refraction. The incident light, the reflected light, and the refracted light lie on the same plane as incidence plane, the reflected light can be worked out by Fresnel Equations, it predicts the intensity ratio of the reflected light to that of the incident light, this ratio is called reflectance [29].

$$R = \frac{I_r}{I_o} \quad (1.10)$$

Here, R is the reflectance of light, I_r is the intensity of the reflected light, and I_0 is the intensity of incident light. If the incident light is polarized perpendicular to the plane of incident, the reflectance is,

$$R_\perp = \left[\frac{\sin(\theta_i - \theta_t)}{\sin(\theta_i + \theta_t)}\right]^2 \quad (1.11)$$

If the incident light is polarized parallel to the incident plane, the reflectance can be,

$$R_{//} = \left[\frac{\tan(\theta_i - \theta_t)}{\tan(\theta_i + \theta_t)} \right]^2 \quad (1.12)$$

$\perp$ shows the polarized light perpendicular to the plane of incidence, and // polarization parallel to the plane of incidence. θ_i is the angle of incidence , θ_t is the angle of refracted light.

For very small incidence angle, the reflected angle is also very small, so, the approximately,

$$R_{\perp} \approx R_{//} \approx \frac{(n-1)^2}{(n+1)^2} \quad (1.13)$$

In this paper, we have designed an Optical Test Method, which uses Reflectance Anisotropy Spectroscopy (RAS), a normal incidence reflectance technique created by Hinds Instruments, utilizes the anisotropy of reconstructed semiconductor and metal surface, RAS is capable of measuring the difference in incident reflectance $R_{//}$ and $R\perp$ for parallel or perpendicular linearly polarized light[30].

$$\frac{\Delta R}{R} = \frac{R_x - R_y}{(R_x + R_y)/2} \quad (1.14)$$

$$\Delta R = R_{//} - R\perp \quad (1.15)$$

R_x is the x-axis section of the polarization light, R_y is the y-axis section of the polarization light.

2. Experimental

2.1 Sample Preparation

2.1.1 Silicon Wafer Cleaning

This procedure is to remove the contaminants from the silicon wafer surface and to control chemically grown oxide on the silicon wafer surface. First the silicon wafer is cut into 1×1 inch pieces by using diamond cutter and then put in a small beaker, add Methylene Alcohol, sonicate for five minutes, rinse with DI water, and then add NH_4OH (Ammonium Hydro-oxide), H_2O_2(Hydrogen Peroxide) and H_2O (1:1:3) , heat to boiling for 30 minutes, rinse with DI water, add H_2SO_4 (Sulfuric Acid), H_2O_2(Hydrogen Peroxide) and H_2O (1:1:3) , heat to boiling for 30 minutes, rinse with DI water, rinse with hydrofluoric acid (HF) solution for 10 seconds, hydrophobic silicon oxide surface was formed. Dry the silicon wafer with nitrogen gas.

2.1.2 Spin Casting, Samples Annealing and Thickness Measurement

To get various concentrations of EVA (770) and LLDPE solutions, 0.010 – 0.200 g EVA (770) and LLDPE are separately dissolved in 10 ml toluene at room temperature and heated to about 110^0C, to get completely dissolved solutions. After the solution is prepared, we take a clean piece of silicon wafers, it is washed and dried. Place the silicon piece on the spinner and, using a pipette, get enough of the solution to cover the piece of silicon surface, spinner revolute at a rate of 2500 rpm, various thickness thin film of polymer EVA and LLPDE then formed.

These samples are put into an oven under vacuum, increase the temperature from the room temperature to 120^0C (for EVA770 samples) or 140^0C (for LLPDE samples) gradually, stay at that temperature for one hour, and slowly drop the temperature to room temperature.

Ellipsometer is used for measuring the thickness of polymer film. It uses the monochromatic wavelength of light either red, blue, or violet, shining on a material, capturing the reflection, the analysis is dependent on Snell's law.

2.2 Differential Scanning Calorimetry (DSC)

Differential Scanning Calorimetry (DSC) is a technique to measure the energy necessary to maintain no difference between the amount of heat required to increase the temperature of a sample and a reference material. Both the sample and reference material are kept at the same temperature environment when heated and cooled at a controlled rate.

In this experiment, a heat-flux type (Model DSC831E by Mettler-Toledo Instrument) is applied. 12mg EVA (770) or 13mg LLPDE are measured from 30^0C to 150^0C, with heating rate 3^0C/min, and under dry nitrogen atmosphere.

2.3 Atomic Force Microscopy (AFM)

Atomic Force Microscope (AFM) is a very high resolution type of scanning probe microscope, AFM provides topographic information down to Angstrom level, with some special probe, it can also obtain other properties such as thermal, electrical conductivity, magnetic characteristics of the sample. Here, different thicknesses (from about 100 Angstrom to more than 1500 Angstrom) of EVA770 and LLPDE films on silicon wafer substrate are measured by the contact mode of AFM. These samples are fixed on the hot plate, which are heated from 330K to 380K for EVA770 and from 340K to 390K for LLPDE at heating rate 1^0C/min. The amplitude of feedback signal changes with temperature is taken, which shows the thermal properties of polymers [31].

SPM (Digital instruments Dimension 3000) is used to measure the topographical image of EVA 770 and LLPDE samples.

2.4 Optical Test Method

Optical Test Method (OTM) is set up to measure the melting characteristics of polymer by polarized light and its interaction with the optical devices.

The OTM includes a laser emitter, a polarizer, a sample holder, a photo-elastic modulator (Hinds PEM-90^{TM}), a piece of Kapton, a second polarizer called an analyzer and a photo-detector, as shown in Figure 2. The analyzer is oriented 90º to the first

polarizer, PEM is oriented 45^{o} to the first polarizer, as the laser light ejected from the laser emitter passes through polarizer, PEM, the sample, the kapton and the analyzer, the output beam involves time-varying birefringence of all devices and polymer films.

A polarizer is a filter that only allows light with a specific orientation to pass through it. In this experiment, two linear polarizers are applied.

PEM is an optical device used to modulate the polarization of an input light, the photo-elastic effect is used to change the birefringence of the optical element in the photo-elastic modulator. The Hinds PEM-90^{TM} is an instrument used for modulating or varying (at a fixed frequency) the polarization of the beam light. The PEM-90^{TM} includes the Controller, the Electronic Head, and the Optical Head. Its operation is based on the photo-elastic effect, in which mechanically stressed sample exhibits birefringence proportional to the resulting strain.

Based on the Jones Calculus, it is known that the laser beam can be represented by a vector, and the optical device can be showed as Jones Matrix as the follows,

$$[Laser] = I_0 \begin{bmatrix} 1 \\ 0 \end{bmatrix} \quad (2.1)$$

$$[Polarizer] = \begin{bmatrix} 1 & 0 \\ 0 & 0 \end{bmatrix} \quad (2.2)$$

$$[PEM] = \begin{bmatrix} \cos^2 Ae^{i\delta_1/2} + \sin^2 Ae^{-i\delta_1/2} & 2i\sin A\cos A\sin(\delta_1/2) \\ 2i\sin A\cos A\sin(\delta_1/2) & \cos^2 Ae^{-i\delta_1/2} + \sin^2 Ae^{i\delta_1/2} \end{bmatrix}$$

$$= \begin{bmatrix} Q_{11} & Q_{12} \\ Q_{21} & Q_{22} \end{bmatrix} \quad (2.3)$$

$$[Sample] = \begin{bmatrix} \cos^2 Be^{i\delta_2/2} + \sin^2 Be^{-i\delta_2/2} & 2i\sin B\cos B\sin(\delta_2/2) \\ 2i\sin B\cos B\sin(\delta_2/2) & \cos^2 Be^{-i\delta_2/2} + \sin^2 Be^{i\delta_2/2} \end{bmatrix}$$

$$= \begin{bmatrix} M_{11} & M_{12} \\ M_{21} & M_{22} \end{bmatrix} \quad (2.4)$$

$$[Kapton] = \begin{bmatrix} \cos^2 C e^{i\delta_3/2} + \sin^2 C e^{-i\delta_3/2} & 2i \sin C \cos C \sin(\delta_3/2) \\ 2i \sin C \cos C \sin(\delta_3/2) & \cos^2 C e^{-i\delta_3/2} + \sin^2 C e^{i\delta_3/2} \end{bmatrix}$$

$$= \begin{bmatrix} N_{11} & N_{12} \\ N_{21} & N_{22} \end{bmatrix} \quad (2.5)$$

$$[Analyzer] = \begin{bmatrix} 0 & 0 \\ 0 & 1 \end{bmatrix} \quad (2.6)$$

B, C are the azimuths of the sample and kapton, δ_2, δ_3 are the retardations of sample and kapton, Q_{ij}, M_{ij} and N_{ij} represent their elements of Jones Matrix, they are constants in this experiment. A is the azimuth of PEM, δ_1 is the sinusoidal retardations of PEM, and it can be represented as

$$\delta_1 = \delta_0 \sin(\omega t) \quad (2.7)$$

Here δ_0 is amplitude of retardation and ω is the oscillation frequency of PEM.

$$[I'] = [Analyzer][Kapton][Sample][PEM][Polarizer][Input\,Light]$$

$$= \begin{bmatrix} 0 & 0 \\ 0 & 1 \end{bmatrix} \begin{bmatrix} N_{11} & N_{12} \\ N_{21} & N_{22} \end{bmatrix} \begin{bmatrix} M_{11} & M_{12} \\ M_{21} & M_{22} \end{bmatrix} \begin{bmatrix} Q_{11} & Q_{21} \\ Q_{21} & Q_{22} \end{bmatrix} \begin{bmatrix} 1 & 0 \\ 0 & 0 \end{bmatrix} \begin{bmatrix} 1 \\ 0 \end{bmatrix} I_0$$

$$= I_0 \begin{bmatrix} 0 \\ (M_{11}N_{21} + M_{21}N_{22})(\cos^2 A e^{i\delta_1/2} + \sin^2 A e^{-i\delta_1/2}) + 2(M_{12}N_{21} + M_{22}N_{22}) i \sin A \cos A \sin(\frac{\delta}{2}) \end{bmatrix}$$

(2.8)

$$\left[I^{'}\right]=\begin{bmatrix} I_x^{'} \\ I_y^{'} \end{bmatrix} \quad (2.9)$$

Since $I_r = RI^{'}$ (2.10),

$$\left[I_r\right]=\begin{bmatrix} I_x^{'} \\ I_y^{'} \end{bmatrix} = R\begin{bmatrix} I_x^{'} \\ I_y^{'} \end{bmatrix} \quad (2.11)$$

$$\left[I_r\right] = R\begin{bmatrix} I_x^{'} \\ I_y^{'} \end{bmatrix}$$

$$= RI_0\begin{bmatrix} 0 \\ (M_{11}N_{21}+M_{21}N_{22})(\cos^2 Ae^{i\delta_1/2}+\sin^2 Ae^{-i\delta_1/2})+2(M_{12}N_{21}+M_{22}N_{22})i\sin A\cos A\sin(\frac{\delta}{2}) \end{bmatrix}$$

(2.12)

$$I_{r-x} = 0 \quad (2.13)$$

$$I_{r-y} = RI_o[(M_{11}N_{21}+M_{21}N_{22})(\cos^2 Ae^{i\delta_1/2}+\sin^2 Ae^{-i\delta_1/2})+2(M_{12}N_{21}+M_{22}N_{22})i\sin A\cos A\sin(\frac{\delta}{2})]$$

(2.14)

It is defined that,

$$Vdc = RI_0(M_{11}N_{21}+M_{21}N_{22})(\cos^2 Ae^{i\delta_1/2}+\sin^2 Ae^{-i\delta_1/2}) \quad (2.15)$$

$$V1f = 2RI_0(M_{12}N_{21}+M_{22}N_{22})i\sin A\cos A\sin(\frac{\delta}{2}) \quad (2.16)$$

Vdc and V1f are measured by voltmeters connected to a photo-detector, which is connected with the modulating frequency of PEM.

3 Experimental Results

3.1 DSC Experiment

Figure 3 and Figure 4 are schematic DSC curves of EVA (770) and LLPDE, which demonstrate their melting features. The endothermic peaks in the DSC curves show the melting temperature of tested materials. As we can see in Figure 3, the melting temperature of EVA770 is about 97^0C, and in Figure 4, the melting temperature of LLPDE is about 115^0C.

3.2 Atomic Force Microscopy

Atomic Force Microscopy (AFM) contains a certain thermal sensing probe with a thermal-couples stage used to measure the melting temperature of polymer films. The melting temperature can be deduced from the vertical motion as the probe sinks into the polymer film below, and it can be represented as light signal amplitude transition from the curve recorded.

Figure 5 to figure 14 are schemes show Amplitude Vs Temperature of EVA 770 by AFM for different thickness films, from thin to relatively thick film (146Å to 1688Å). As we can see that all the curves show good transitions while going melting process, the melting point of film with thickness 146 Å is about 351K(78^0C), while the melting temperature of film with thickness 1400Å is about 372.5K (99.5^0C), there are nearly 21.5K maximum difference between the thin and thick EVA770 films we tested. Also, it is noticed that the melting temperature of EVA770 increase gradually with the increasing thickness, as in Table 3 and figure 15. Below thickness of 416Å, the change of melting temperature is not large, above 863Å, the change is not large either, and it researches almost stable about 370K.

For LLPDE films, Figure 16 to 23 indicate Amplitude Vs Temperature by AFM , for film with thickness 140 Å, the melting temperature is 370K, and for thickness 1504 Å, the melting temperature is about 395K, the gap is 25K.

Figure 25 are scanning probe microscope (SPM) topographic images of EVA770 annealed samples, with thickness 230 Å, 650 Å and 1215 Å, film of 1215 Å shows spherulite structure. As the film thickness decreases, the structure becomes coarse and large dendrite crystals for 650 Å, and thin and small dendrite crystals for thickness 230Å. Figure 26 are topographic images of LLPDE annealed samples by SPM with thickness 323 Å, 616 Å, 1087Å. The thick LLPDE film of 1807 Å is like spherulite and dendrite together, the structure of thickness 616 Å is coarse dendrite shape, and 323 Å thickness sample is thin dendrite shape.

3.3 Optical Test Method

Optical Test Method is using a polarized light incidence reflectance technique, which measures the light information change due to the optically isotropy of the materials.

Figure 27 is a general heating and cooling process of EVA sample in this experiment (take sample EVA770 with thickness 1866Å for an example). The heating rate is about 2.2^0C/min. Figure 28 and Figure 29 are V1f and Vdc vs. time of EVA 770 with thickness 1866Å, as we can see that, at the beginning, V1f and Vdc increase a little, and then experience a dramatic descending process. After some stable period, there is a abrupt increasing curve, at last, reach at a stable stage.

From Figure 33 to Figure 46, the variation characteristics of V1f and Vdc with temperature for different thickness EVA 770 are plotted separately. For each sample, there are two dramatic transitions, the descending and the increasing in short time. The descending point shows the melting temperature, while the increasing point represents the re-crystallization temperature. Comparing the samples with thickness 116 Å to 1866 Å, the melting temperature for 116 Å is about 72^0C (345K), while the melting temperature of 1866 Å sample is about 95^0C (368K). There is a 23K gap between them. Also the melting temperature of different thickness EVA 770 increases as the thickness increases until reaches the bulk film melting temperature.

Figure 30 indicates the heating and cooling process of LLPDE sample in this experiment (take sample with thickness 1412Å for an example), the heating rate is about

2.2^0C/min, the change behavior of V1f and Vdc vs. time is similar to that of EVA 770 as above mentioned, shown in Figure 31 and Figure 32.

Figure 48 to Figure 59 display the variation characteristics of V1f and Vdc with temperature for different thickness from 182 Å to 1412 Å of LLPDE, similarly, two dramatic changes occured, the descending and the increasing transition. The melting temperature for 182 Å is about 90^0C (363K), while the melting temperature of 846 Å sample is about 112^0C (385K), the maximum gap is about 22^0C (K).

4 Discussions and Conclusions

4.1 Discussions

Among many theoretical studies that define the characteristics of the melting temperature of polymer films, two methods are universally applied, which are Gibbs-Thomson Equation and Hoffman-Weeks Methods. Gibbs-Thomson Equation describes the relationship between the melting temperature and lamellar thickness of polymer film thermodynamically [32, 33].

$$T_m(l) = T_m^o - \frac{C}{l} \quad (4.1)$$

Where T_m^0 is the melting temperature of an infinite edge polymer, $T_m(l)$ is the melting temperature of polymer lamellar with thickness l, C is a constant depends on the properties of polymer, l is thickness of polymer lamellar. From Gibbs-Thomson Equation, we know that, under certain circumstance, the melting temperature of polymer film may decrease as the thickness of polymer increases. The Hoffman-Weeks plot method has been widely used to obtain T_m^0 of polymer films, it is based on Gibbs-Thomson Equation and the surface nucleation theory.

In this paper, T_m^0 is determined by Differential Scanning Calorimetry (DSC), which is about 97^0C for EVA770, and 115^0C for LLPDE, it is compared to the bulk

polymer films measured by AFM and OTM. In AFM experiment, the melting temperature of bulk EVA770 is 372.5K (99.5^{0}C) with thickness 1400Å, while the melting temperature of bulk LLPDE is 395K(122^{0}C) with thickness 1504Å. In OTM experiment, the melting temperature of bulk EVA770 is 368K (95^{0}C) with thickness 1866Å, while the melting temperature of bulk LLPDE is 385K (112^{0}C) with thickness 846Å.

Also it is observed that, for both EVA 770 and LLPDE measured by AFM, the results show similar transition tendency, the melting temperature increases with the thickness, but for the thinner films (less than 400-500 Å), their melting temperatures are close, and also after the thickness reaches certain values (for example, above 800 Å), their melting temperatures can get stable again.

The Optical Test Method (OTM) is designed based on RAS (Reflectance Anisotropy Spectroscopy) Technique provided by Hinds Instrument Inc. including interactions of polarized or polarization modulated light through optical elements and the sample, study the physical properties (here is melting temperature) of the sample by analyzing the reflected light.

Table 5, Figure 47 and Table 6, Figure 60 indicate the OTM experimental results of EVA 770 and LLPDE, both of them show similar variation behavior. There is a large gap of melting temperature when the film thickness is between 100- 400 Å compared with thickness above 800 Å, when the film thickness is below 400 Å or above 800 Å, the melting temperature keep almost stable. The maximum gap of temperature for EVA770 is about 23K, and the maximum gap of temperature of LLPDE is about 22K.

Based on the analysis above, it is shown that for the two main experimental methods studying on the melting temperature of EVA770 and LLPDE films applied in this paper, their results show similar performance, and also agree with the previous statements.

4.2 Conclusions

In this paper, the research is cast on the melting characteristic of two semi-crystalline polymers, poly ethylene vinyl acetate (EVA770) and linear low-density polyethylene (LLDPE), mainly by Atomic Force Microscopy (AFM) and self-designed

Optical Test Method (OTM). Study the relationship between polymer film thickness and melting temperature of EVA 770 and LLPDE, and also investigate the morphology characteristics of polymer thin films after annealing.

The thin and ultra-thin films are spun casting on silicon wafer, after annealing, their melting temperature is measured by Atomic Force Microscopy (AFM) and self-designed Optical Test Method (OTM), results are compared with those of bulk films tested by Differential Scanning Calorimetry (DSC). The AFM and OTM results present similar melting behavior of these two polymer materials, for thin film and ultra-thin film of EVA 770 (from thickness of 116Å to 1866Å) and LLPDE (from thickness of 146Å to 1688`Å), between a given thickness region, the melting temperature increases largely as the thickness increases, above and below a certain film thickness, the melting temperature will show little variation. The maximum melting temperature gap of EVA770 is 21.5K by AFM, and 23K by OTM, while the maximum melting temperature gap of LLPDE is 25K by AFM, and 22K by OTM.

In summary, the melting temperature of thin and ultra-thin EVA770 and LLPDE changes largely with the film thickness in a certain zone.

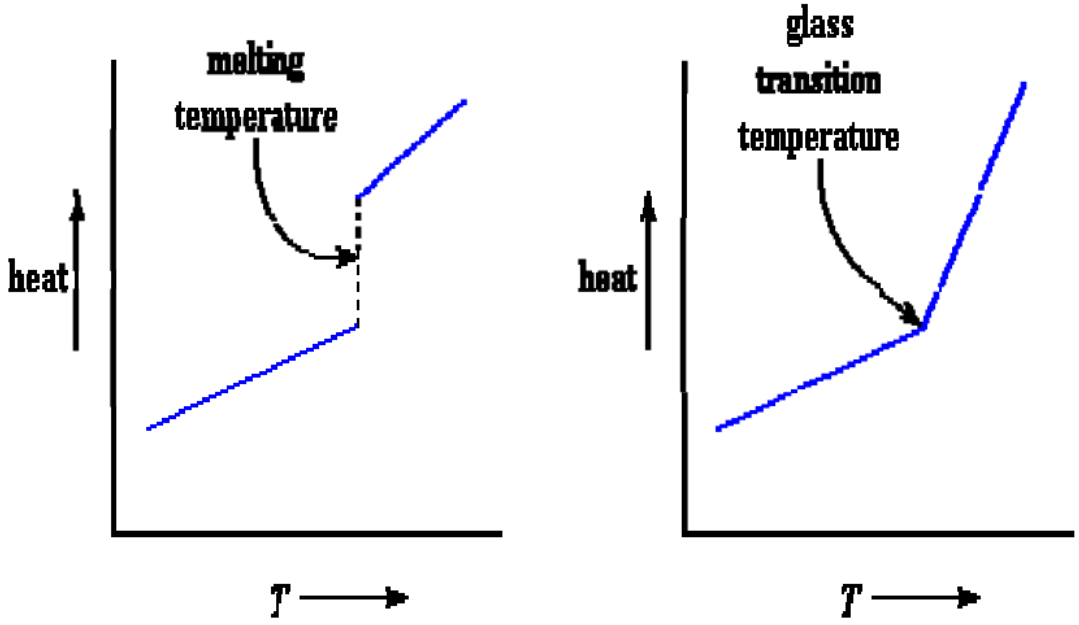

(1) (2)

Figure 1 (1) Heat vs. Temperature for Crystalline Polymer (2) Heat vs. Temperature of Amorphous Polymer

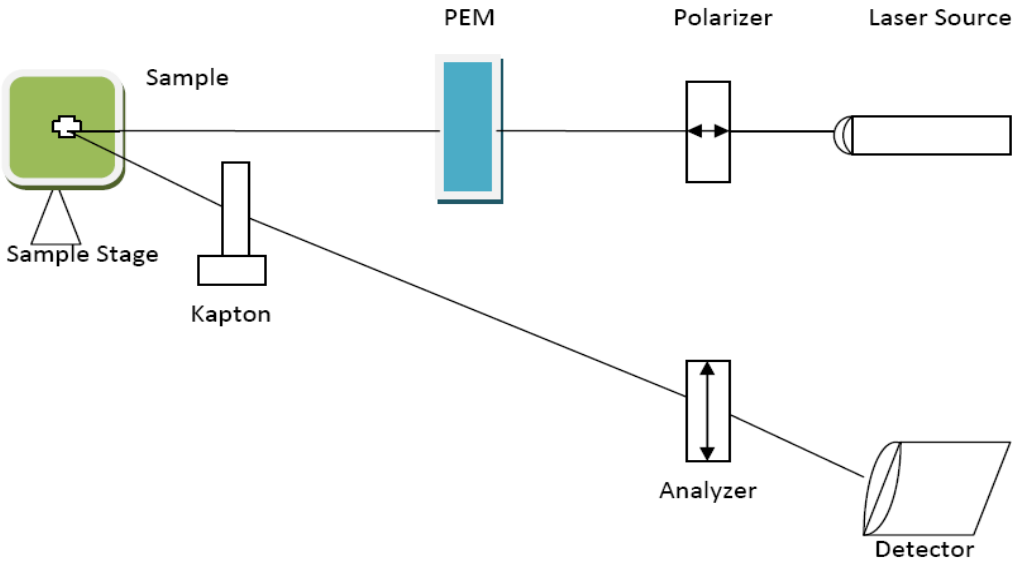

Figure 2 Schematic Diagram of Optical Test Method

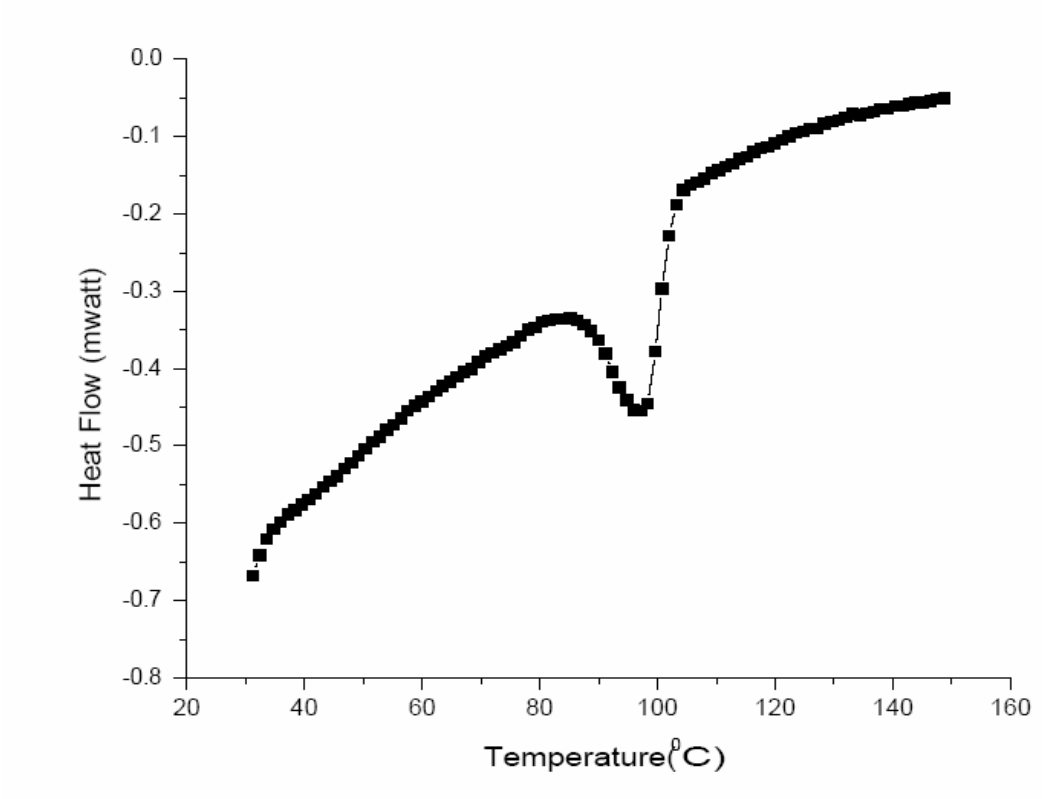

Figure 3 Heat Flow vs. Temperature of EVA770 by DSC

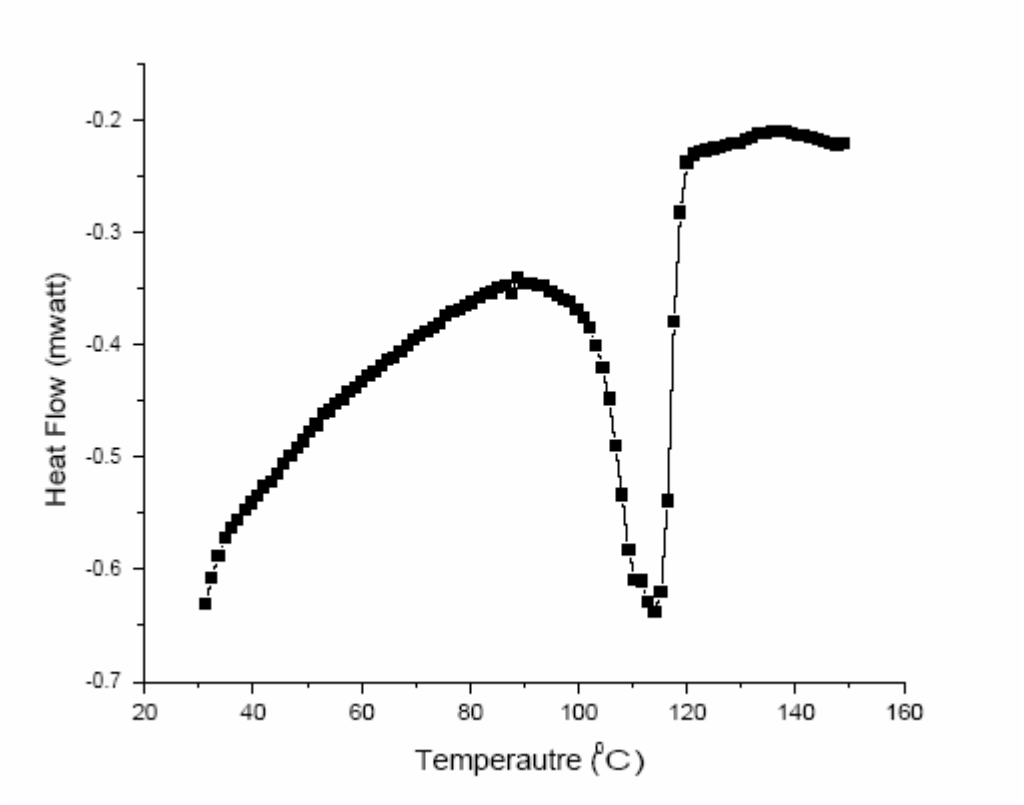

Figure 4 Heat Flow vs. Temperature of LLPDE by DSC

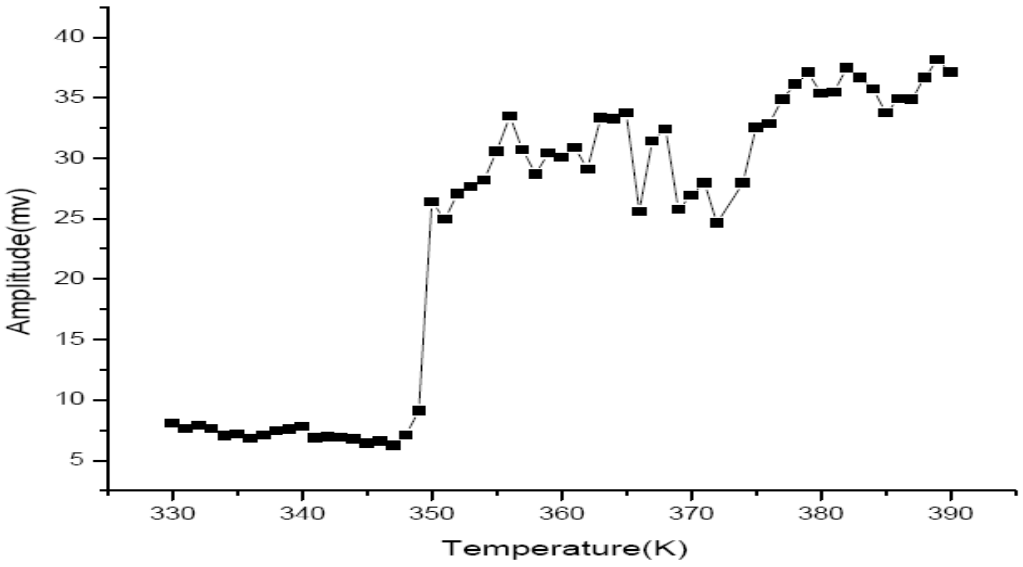

Figure 5 Amplitude vs. Temperature of EVA770 (146Å) by AFM

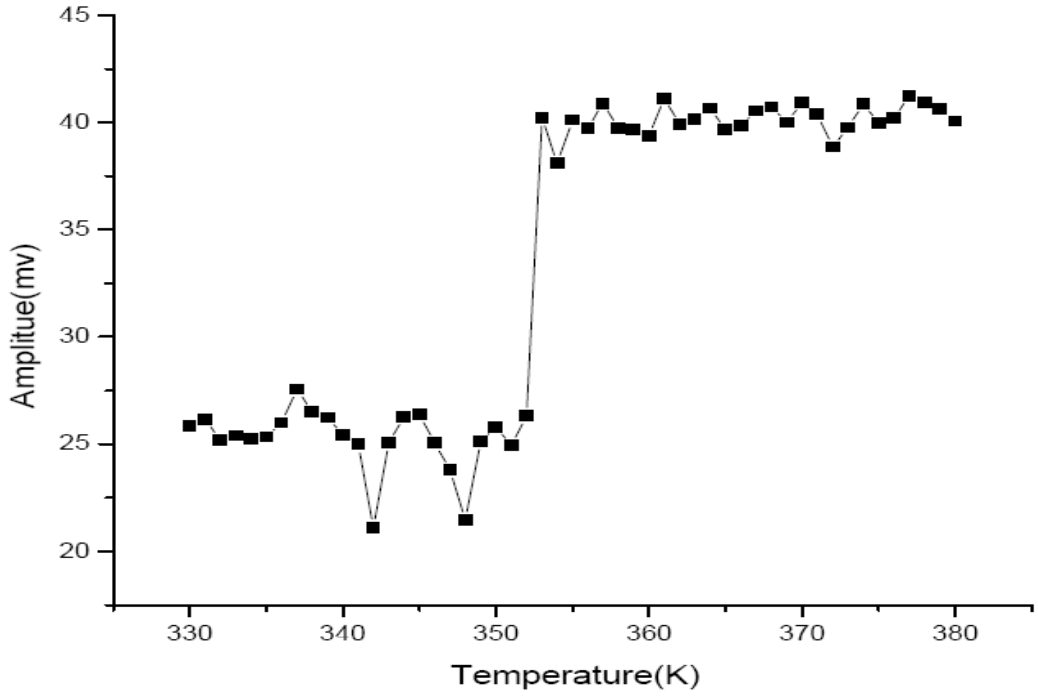

Figure 6 Amplitude vs. Temperature of EVA770 (167Å) by AFM

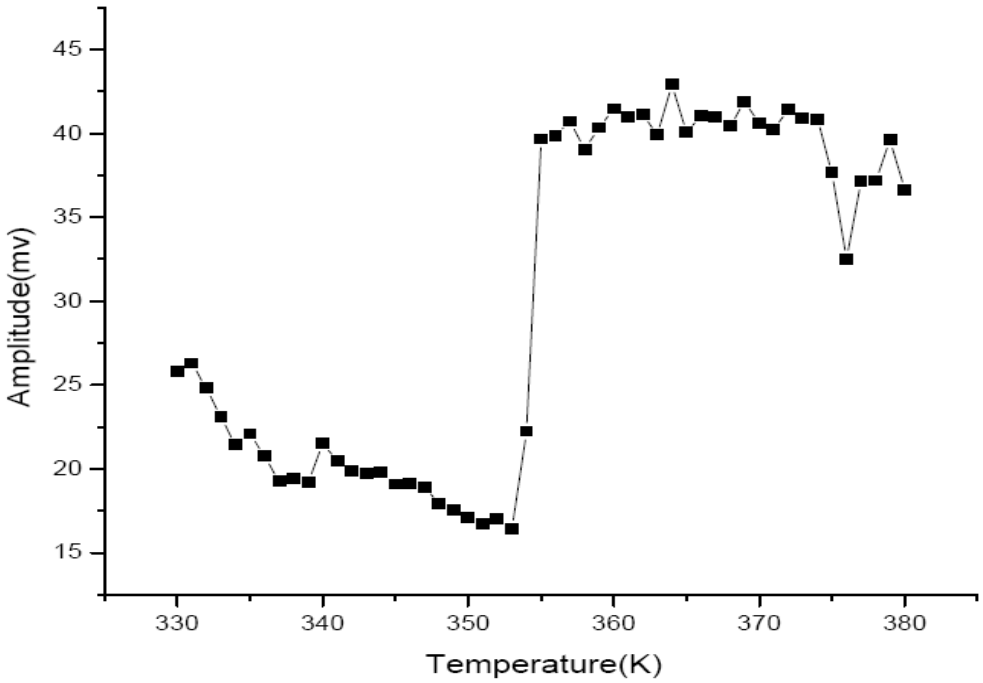

Figure 7 Amplitude vs. Temperature of EVA770 (210Å) by AFM

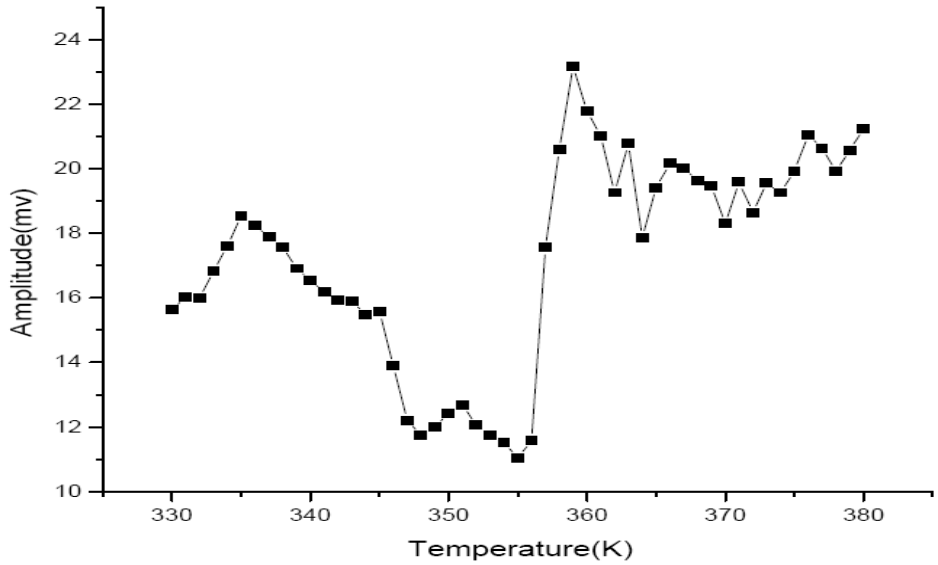

Figure 8 Amplitude vs. Temperature of EVA770 (348Å) by AFM

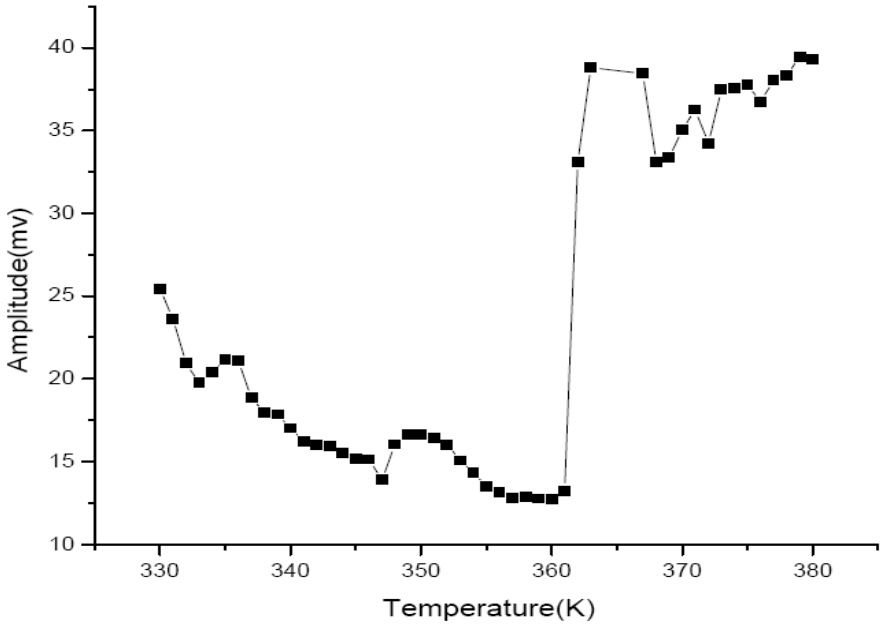

Figure 9 Amplitude vs. Temperature of EVA770 (416Å) by AFM

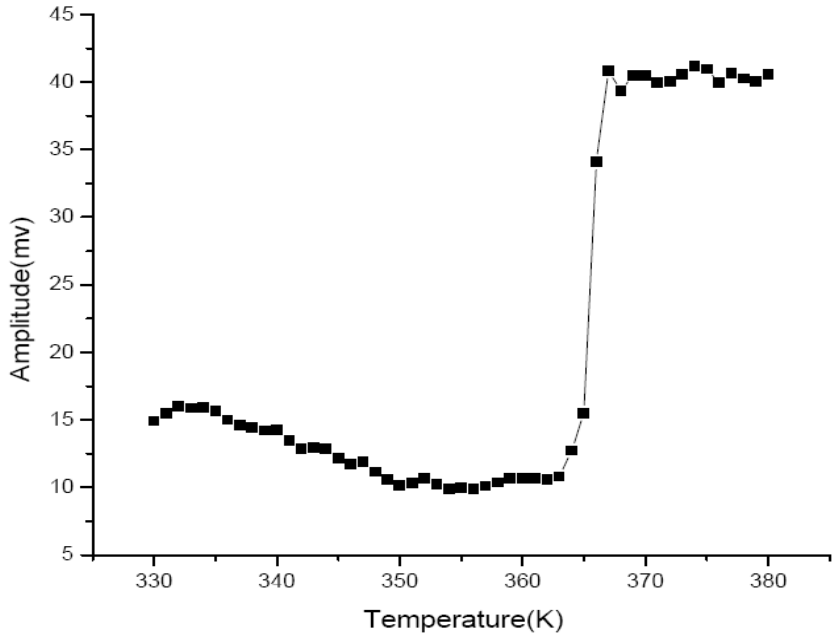

Figure 10 Amplitude vs. Temperature of EVA770 (491Å) by AFM

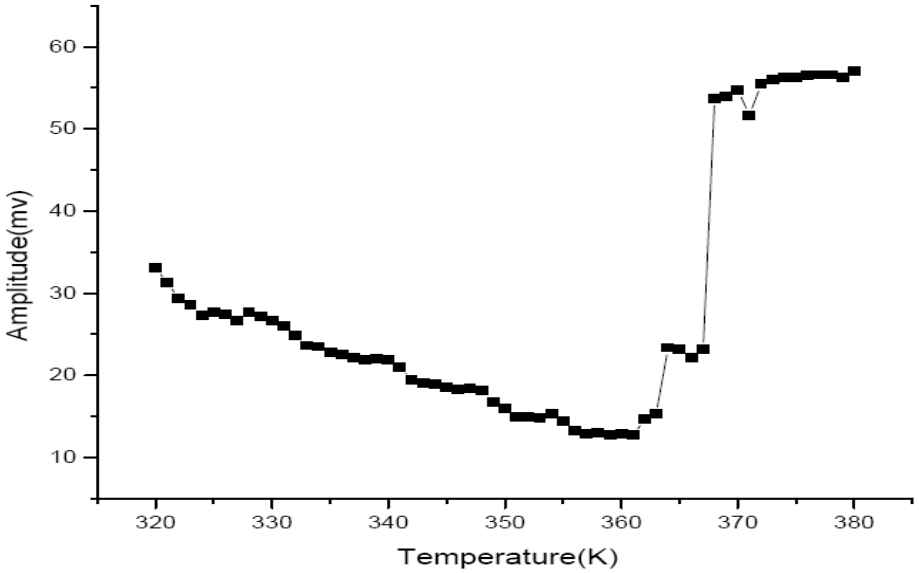

Figure 11 Amplitude vs. Temperature of EVA770 (836Å) by AFM

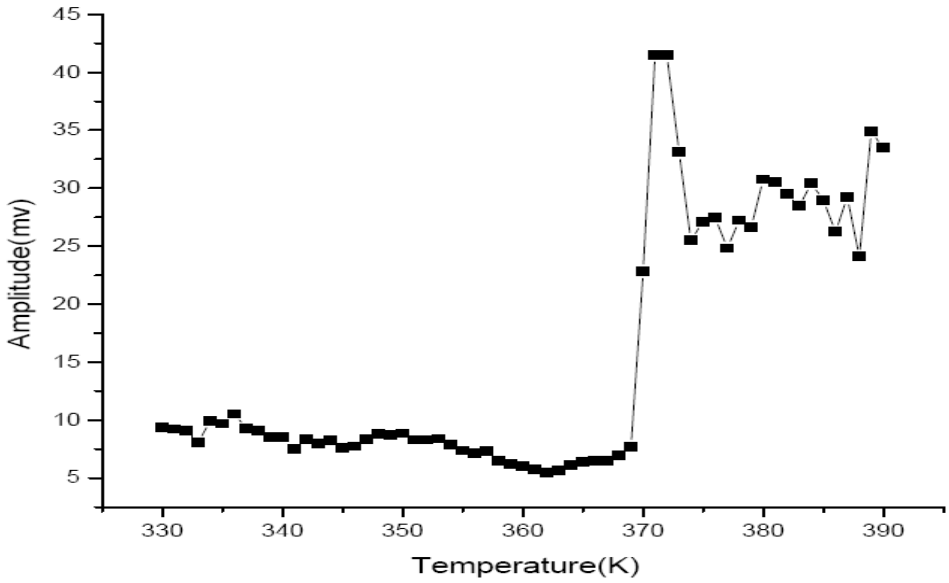

Figure 12 Amplitude vs. Temperature of EVA770 (1211Å) by AFM

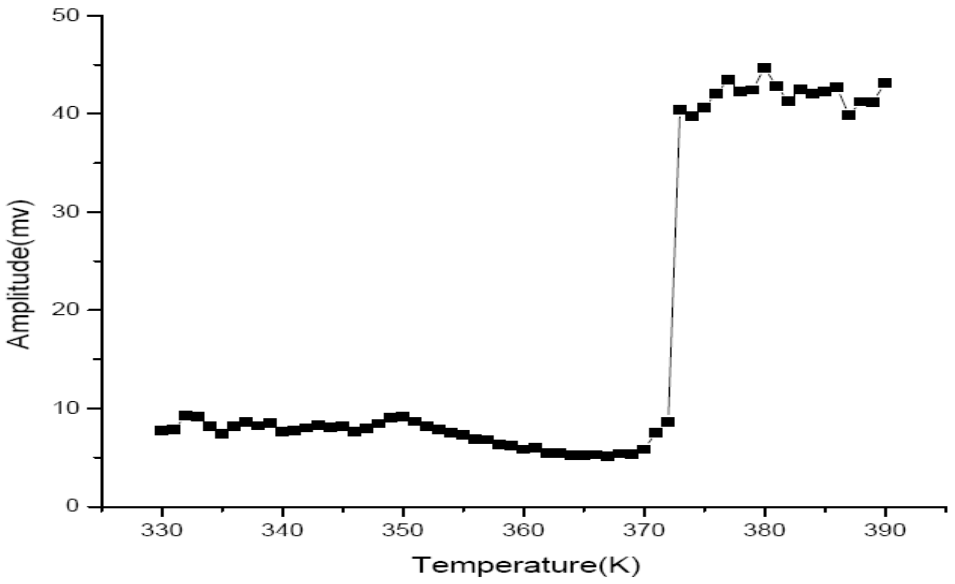

Figure 13 Amplitude vs. Temperature of EVA770 (1400Å) by AFM

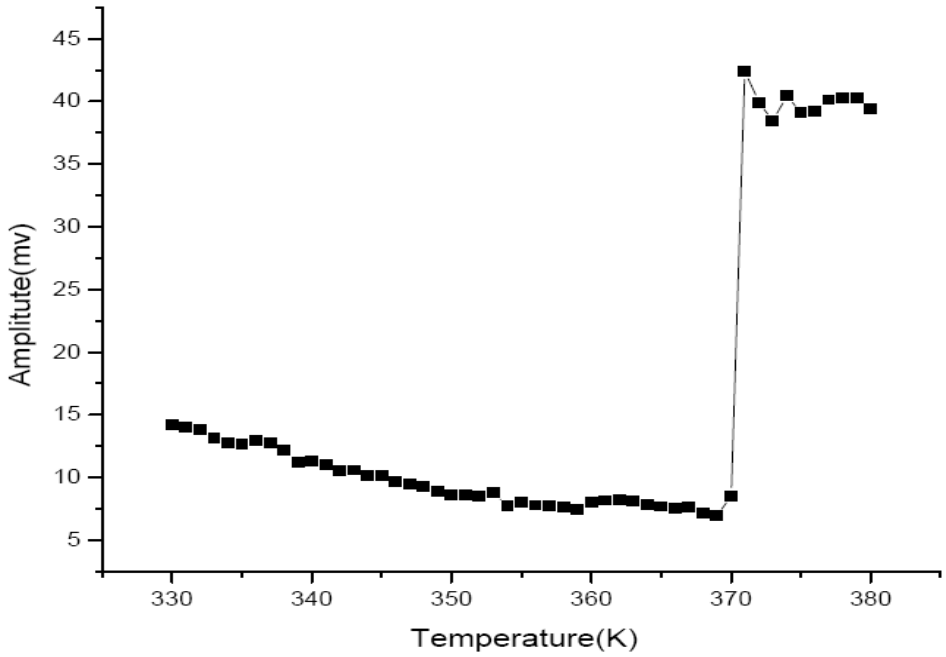

Figure 14 Amplitude vs. Temperature of EVA770 (1688Å) by AFM

Thickness	146Å	167Å	210Å	346Å	416Å	491Å	863Å	1211Å	1400Å	1688Å
Melting Temperature	351K	353K	355K	359K	362K	365.5K	368K	371K	372.5K	371.5K

Table 3 Melting Temperature vs. Film Thickness of EVA770 by AFM

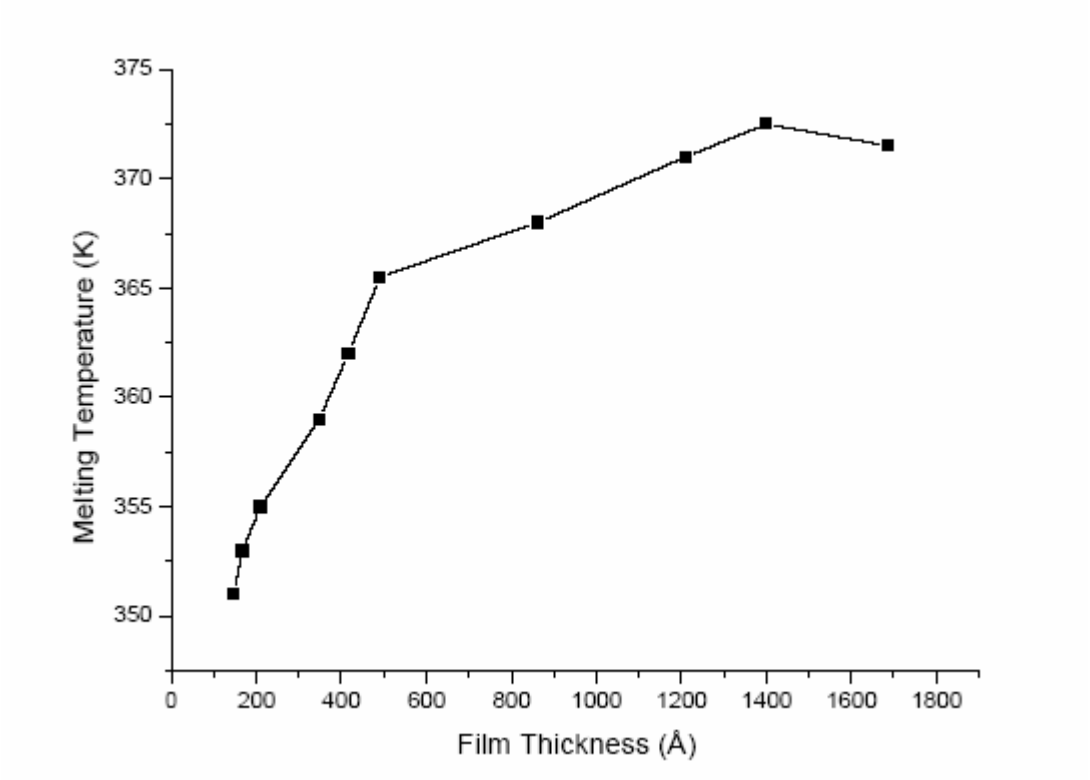

Figure 15 Melting Temperature vs. Film Thickness of EVA770 by AFM

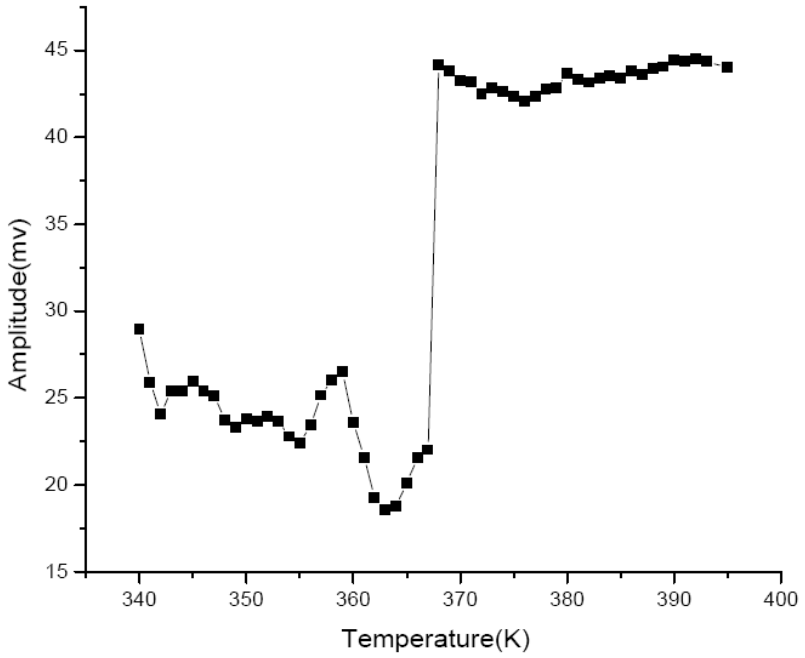

Figure 16 Amplitude vs. Temperature of LLPDE (140Å) by AFM

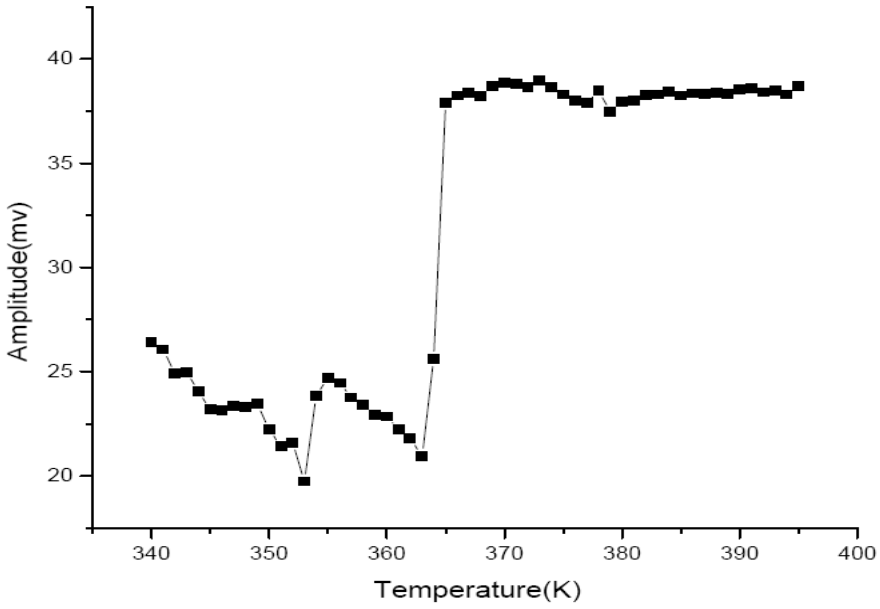

Figure 17 Amplitude vs. Temperature of LLPDE (201Å) by AFM

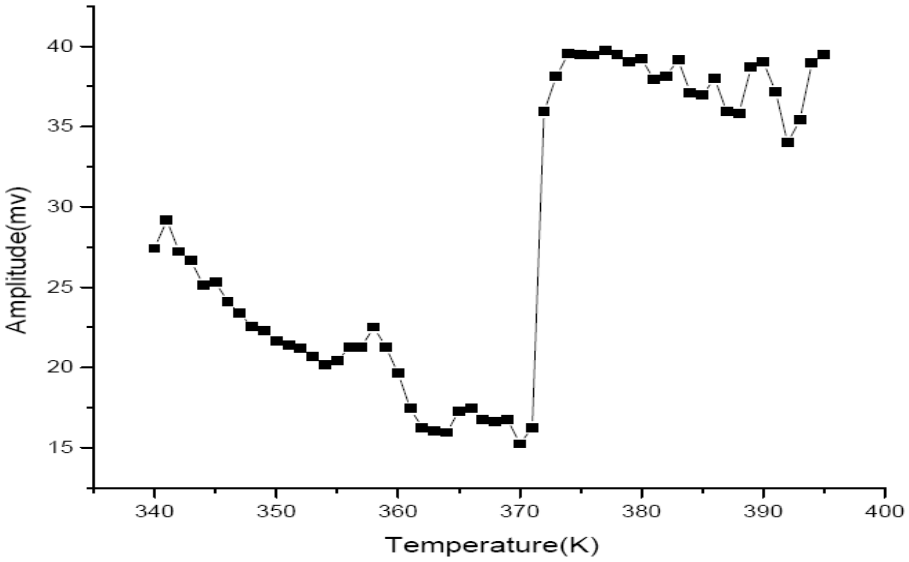

Figure 18 Amplitude vs. Temperature of LLPDE (634Å) by AFM

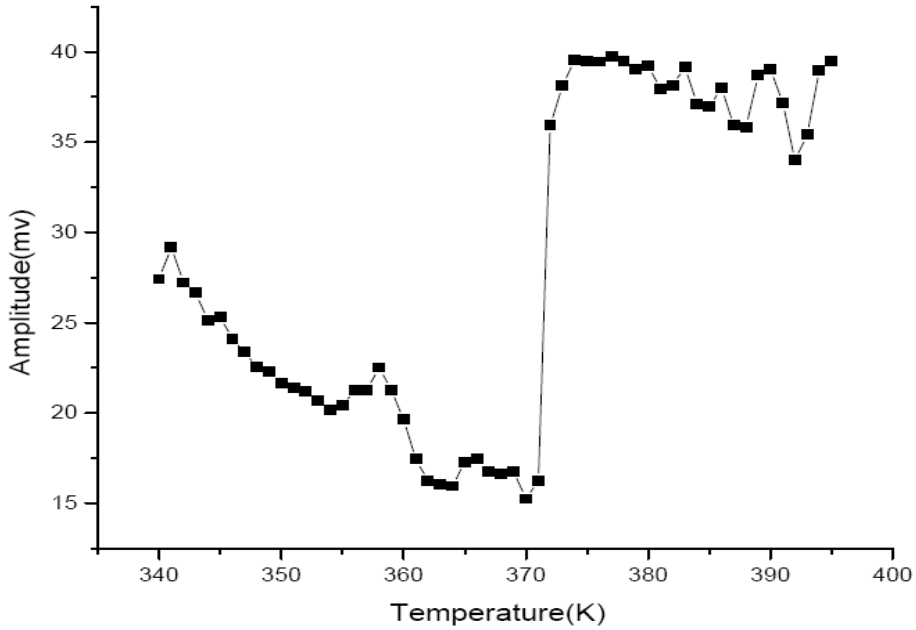

Figure 19 Amplitude vs. Temperature of LLPDE (643Å) by AFM

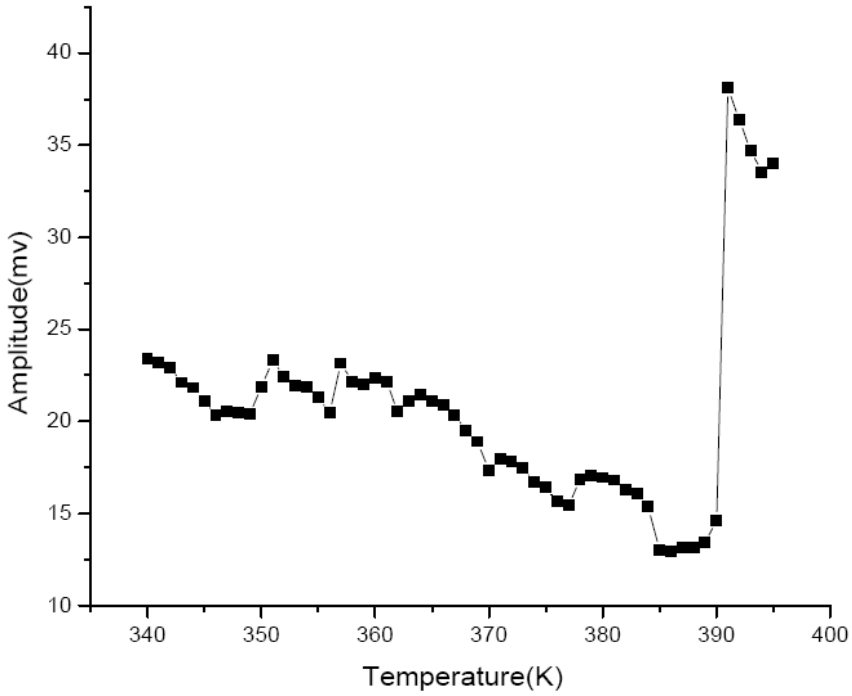

Figure 20 Amplitude vs. Temperature of LLPDE (779Å) by AFM

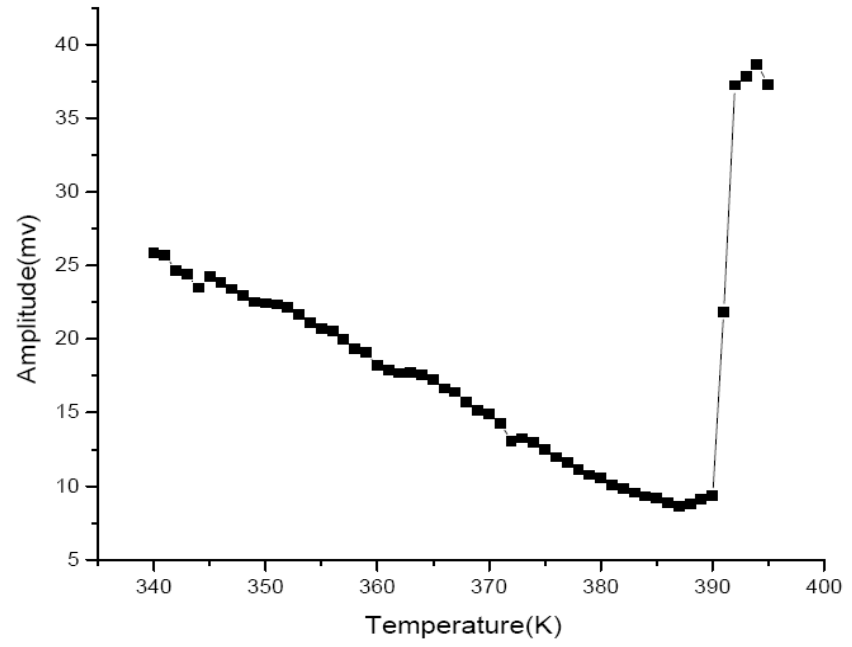

Figure 21 Amplitude vs. Temperature of LLPDE (986Å) by AFM

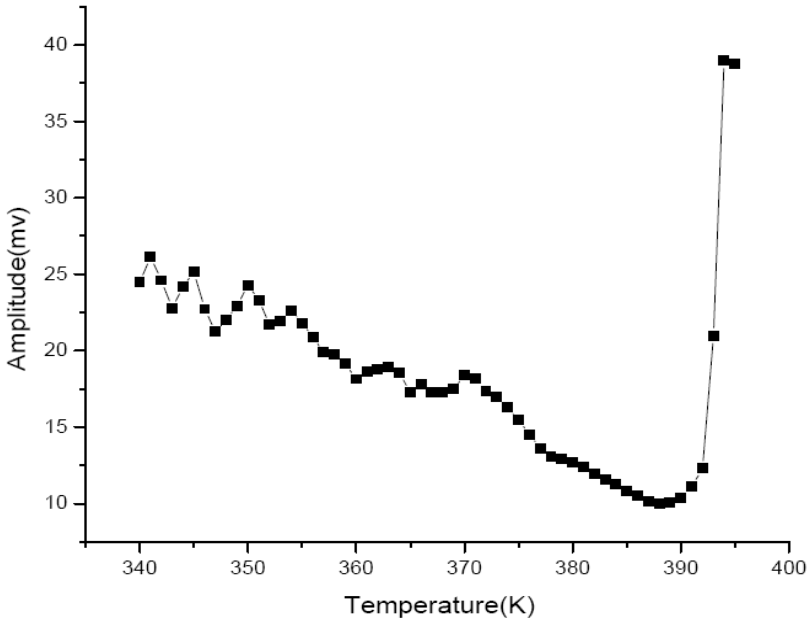

Figure 22 Amplitude vs. Temperature of LLPDE (1132Å) by AFM

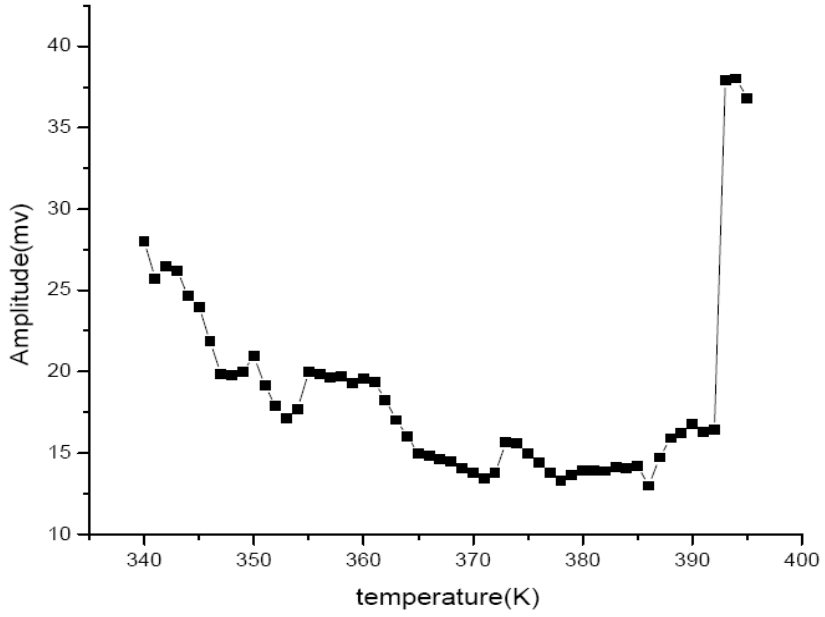

Figure 23 Amplitude vs. Temperature of LLPDE (1504Å) by AFM

Thickness	140Å	201Å	634Å	643Å	779Å	986Å	1132Å	1504Å
Melting Temperature	370K	365.5K	372.5K	372K	392K	392K	394.5K	395K

Table 4 Melting Temperature vs. Film Thickness of LLPDE by AFM

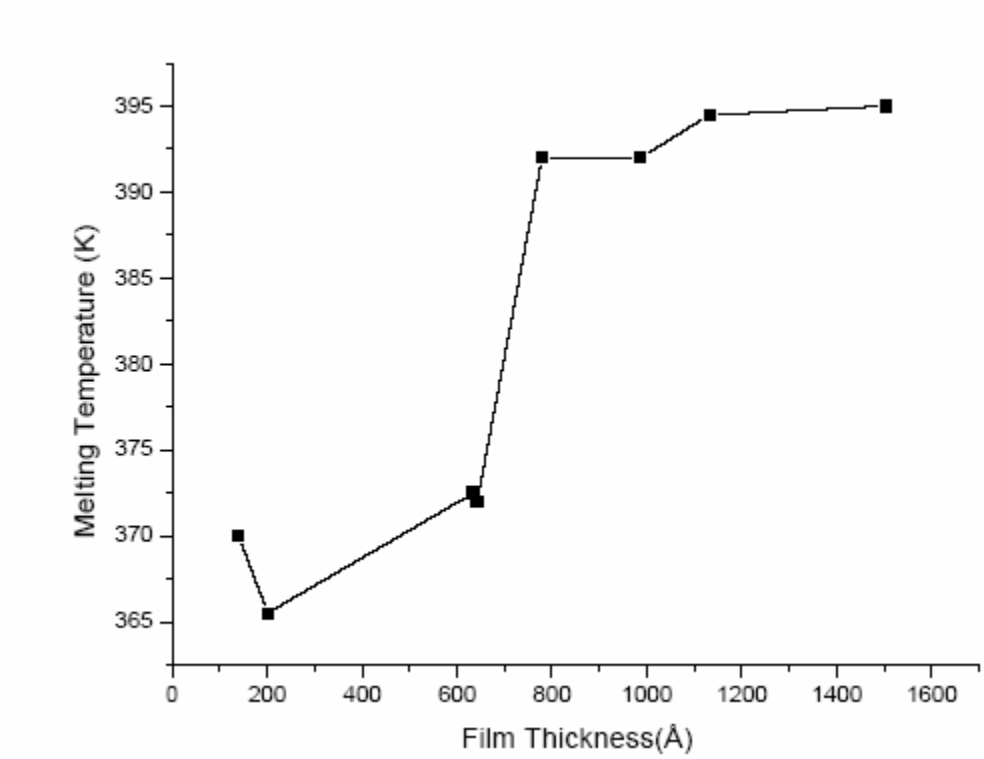

Figure 24 Melting Temperature vs. Film Thickness of LLPDE by AFM

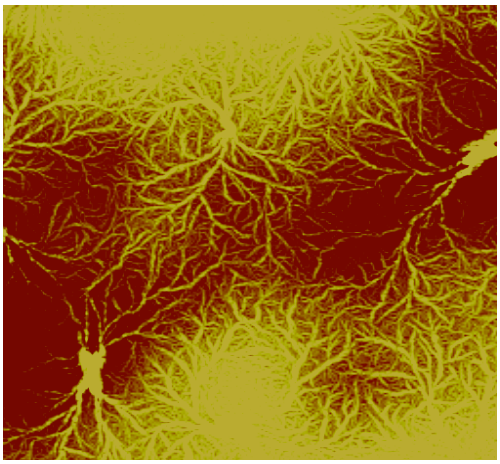

(1) EVA770 (230Å)

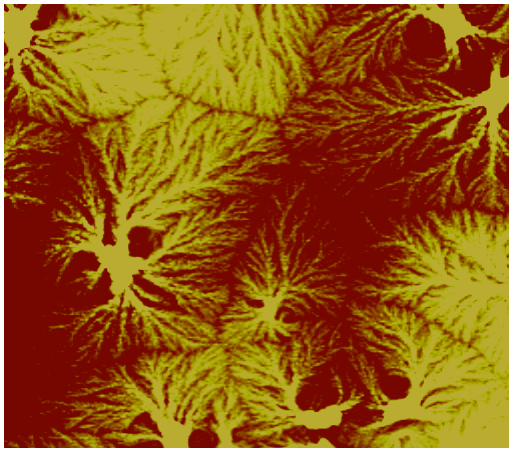

(2) EVA770 (650Å)

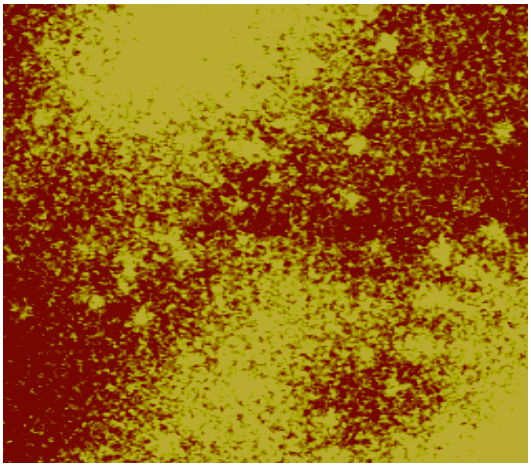

(3) EVA770 (1215Å)

Figure 25 Topographic Images of EVA770 Annealed Samples by SPM, Scan Size 50um

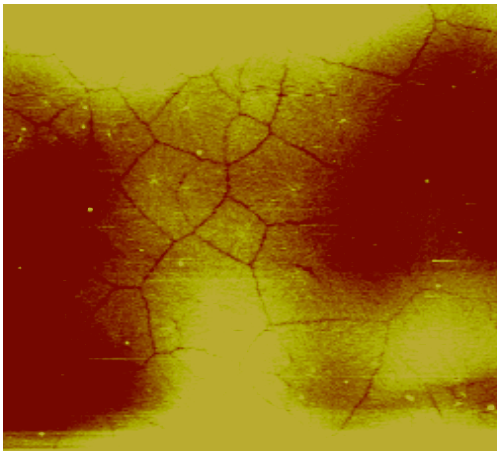

(1) LLPDE (323Å)

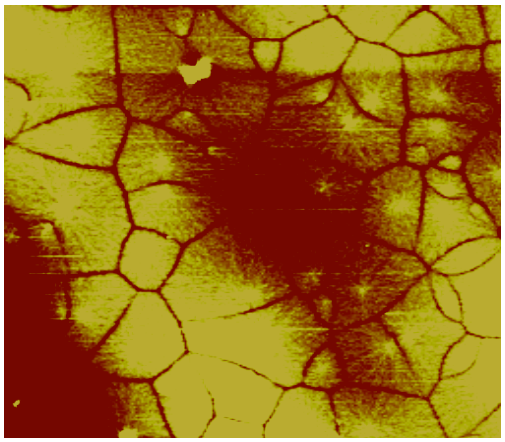

(2) LLPDE (616Å)

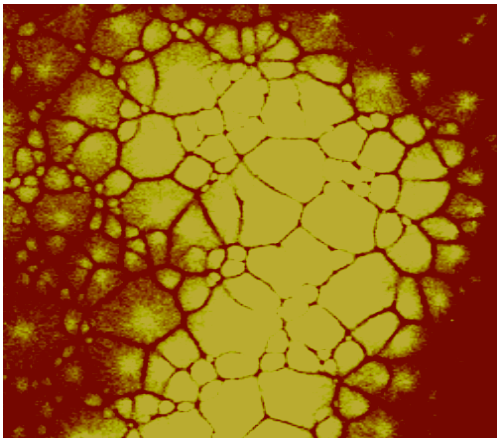

(3) LLPDE (1087Å)

Figure 26 Topographic Images of LLPDE Annealed Samples by SPM, Scan Size 50um

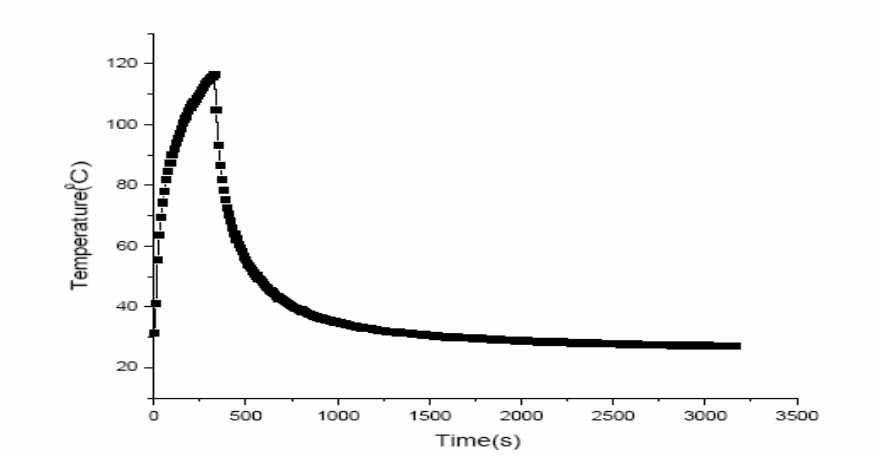

Figure 27 Temperature vs. Time of EVA770 (1866Å) by OTM

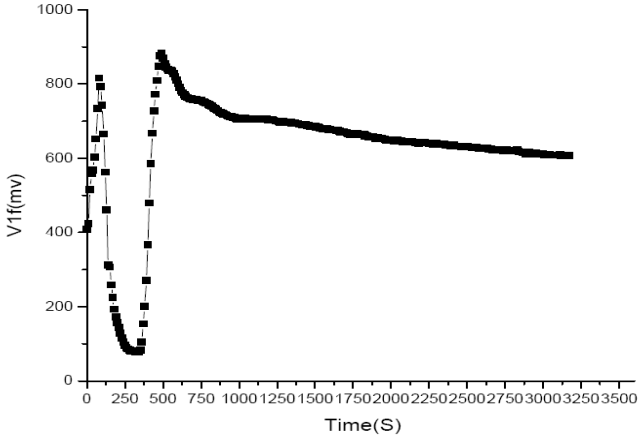

Figure 28 V1f vs. Time of EVA770 (1866Å) by OTM

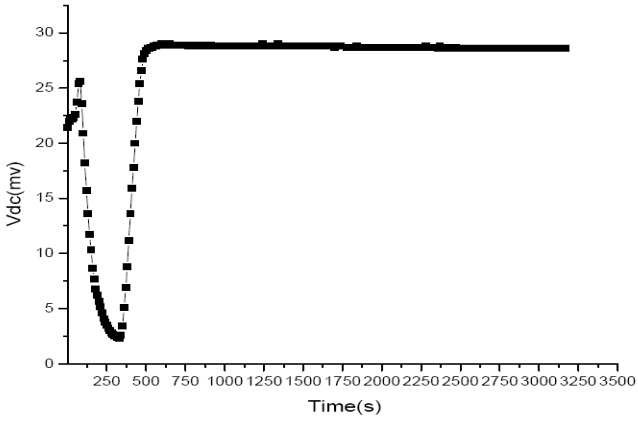

Figure 29 Vdc vs. Time of EVA (1866Å) by OTM

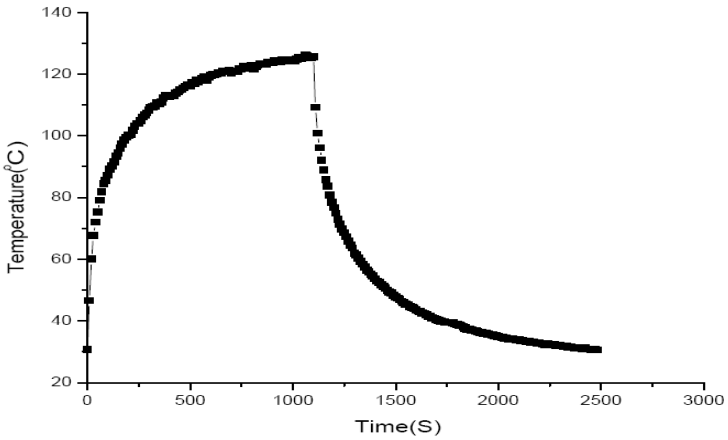

Figure 30 Temperature vs. Time of LLPDE (1412Å) by OTM

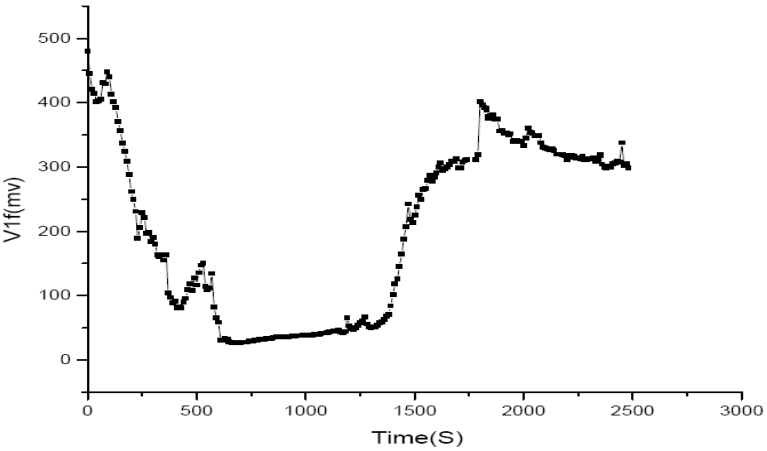

Figure 31 V1f vs. Time of LLPDE (1412Å) by OTM

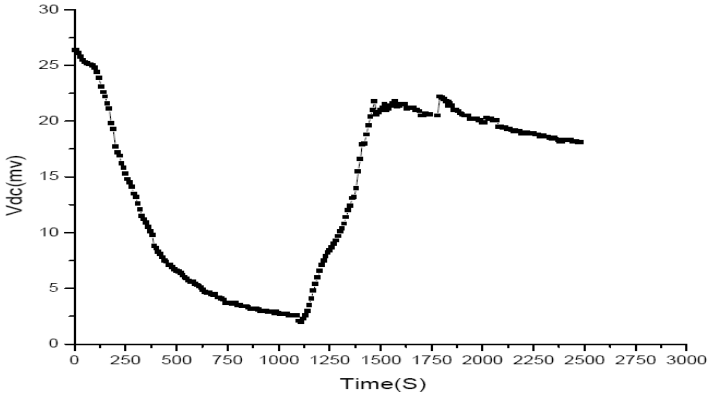

Figure 32 Vdc vs. Time of LLPDE (1412Å) by OTM

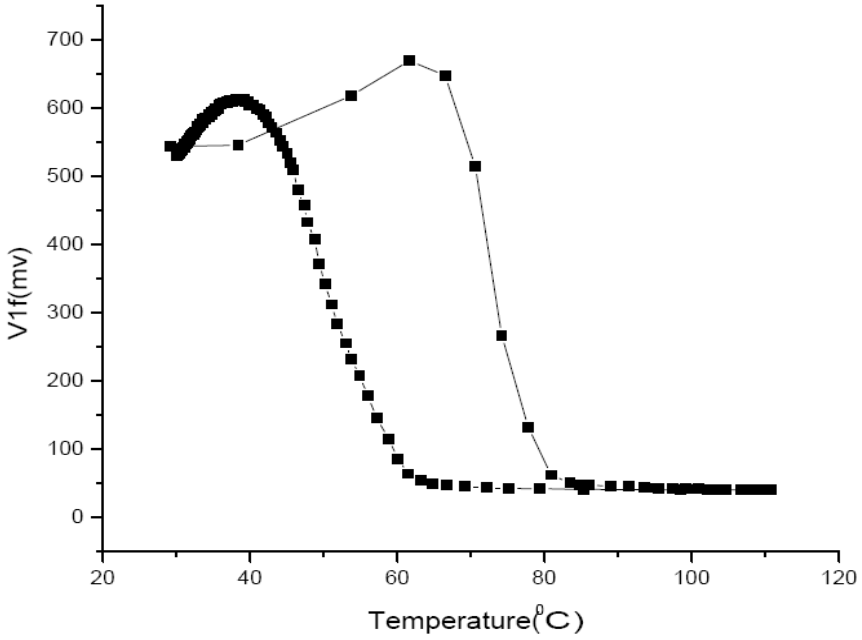

Figure 33 V1f vs. Temperature of EVA770 (116Å) by OTM

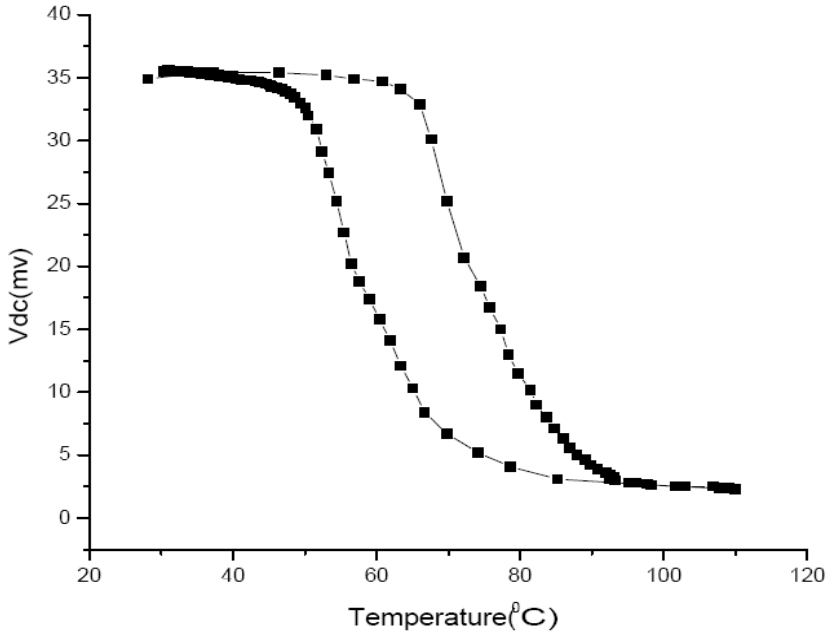

Figure 34 Vdc vs. Temperature of EVA770 (116Å) by OTM

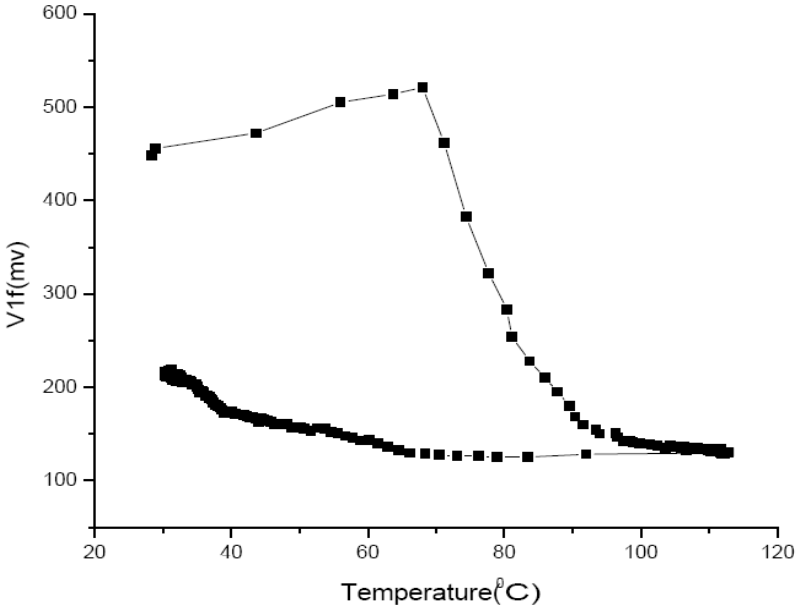

Figure 35 V1f vs. Temperature of EVA770 (262Å) by OTM

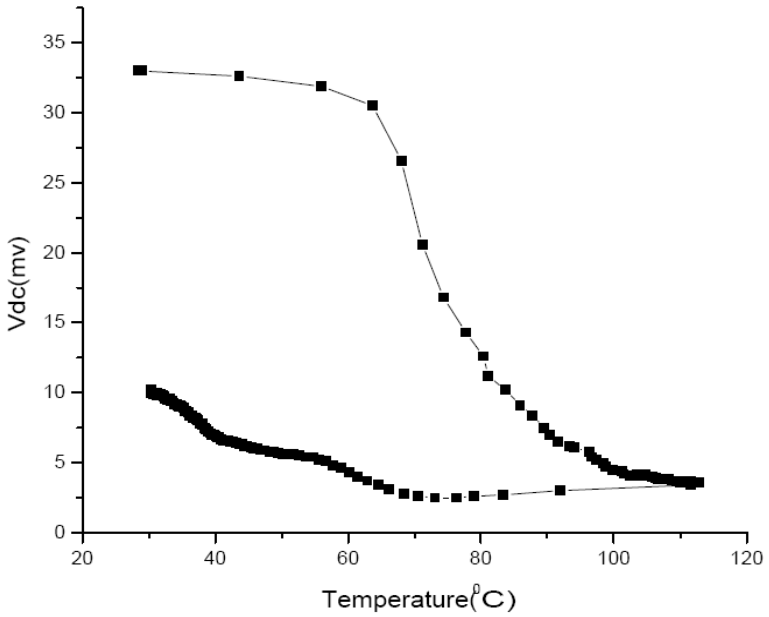

Figure 36 Vdc vs. Temperature of EVA770 (262Å) by OTM

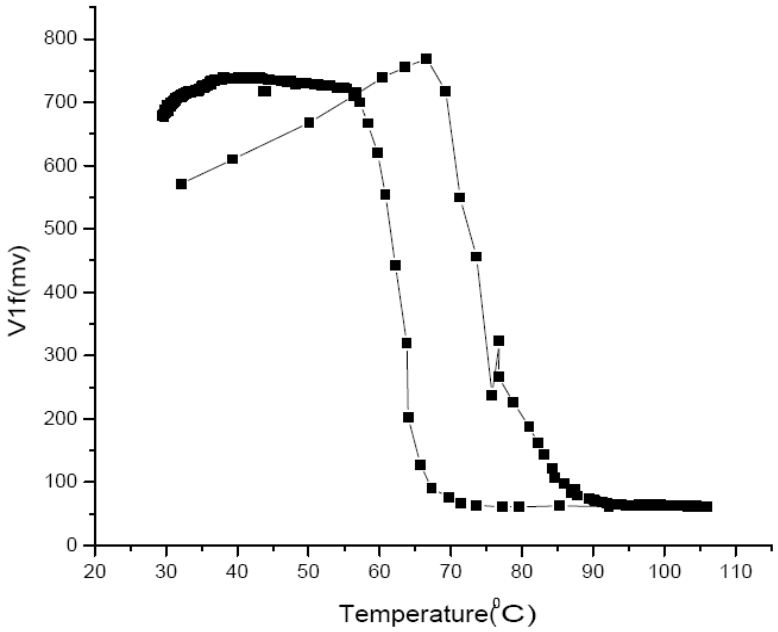

Figure 37 V1f vs. Temperature of EVA770 (352Å) by OTM

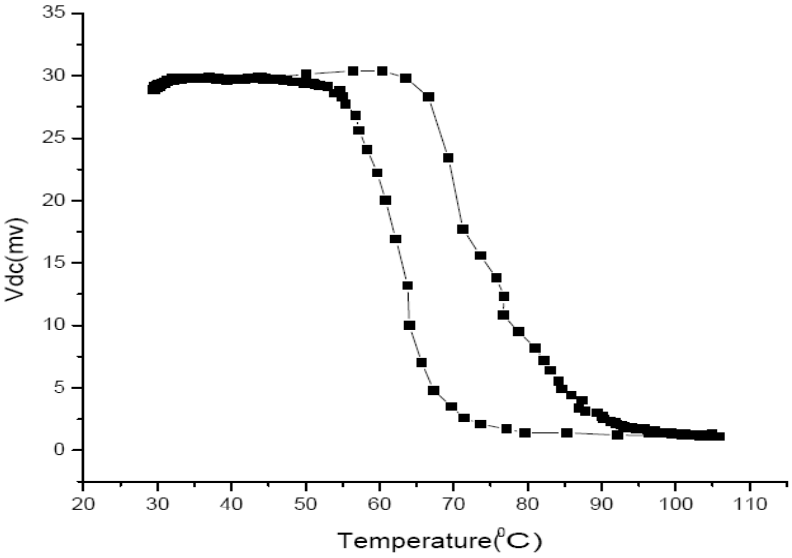

Figure 38 Vdc vs. Temperature of EVA770 (352Å) by OTM

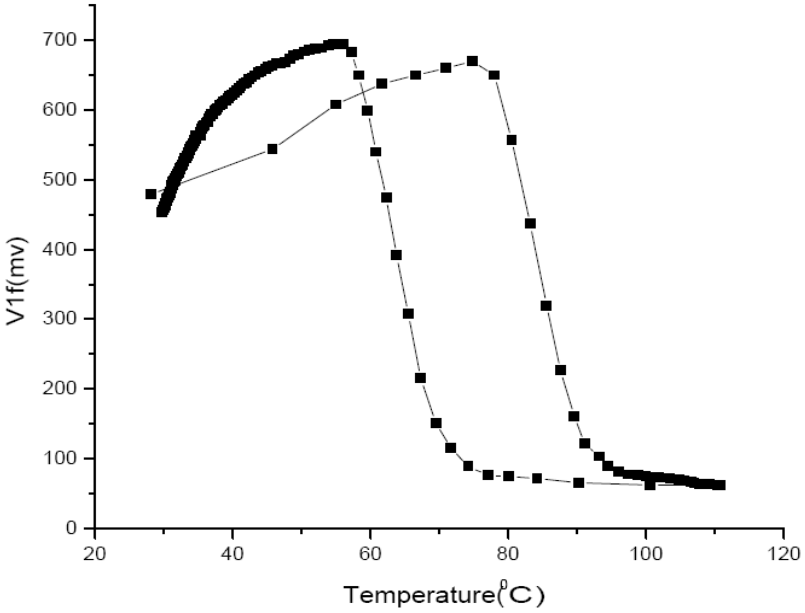

Figure 39 V1f vs. Temperature of EVA770 (431Å) by OTM

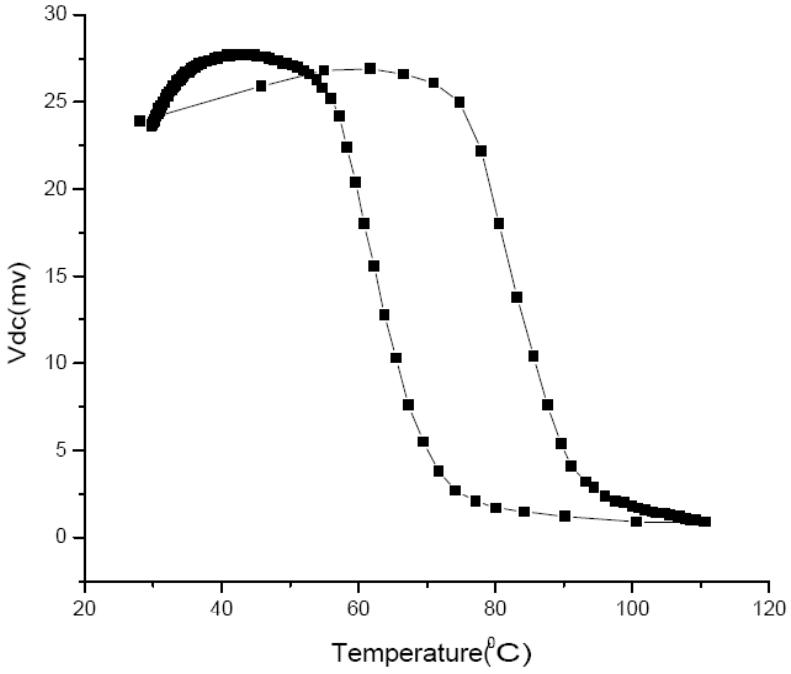

Figure 40 Vdc vs. Temperature of EVA770 (431Å) by OTM

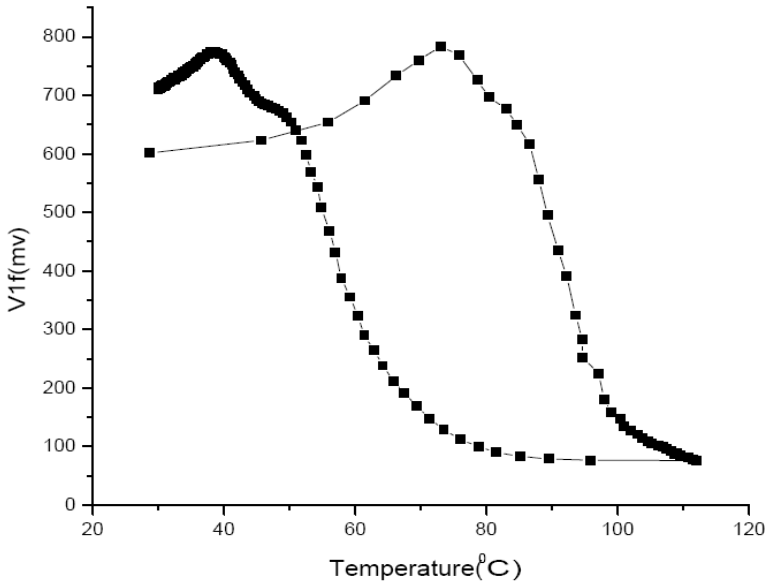

Figure 41 V1f vs. Temperature of EVA770 (613Å) by OTM

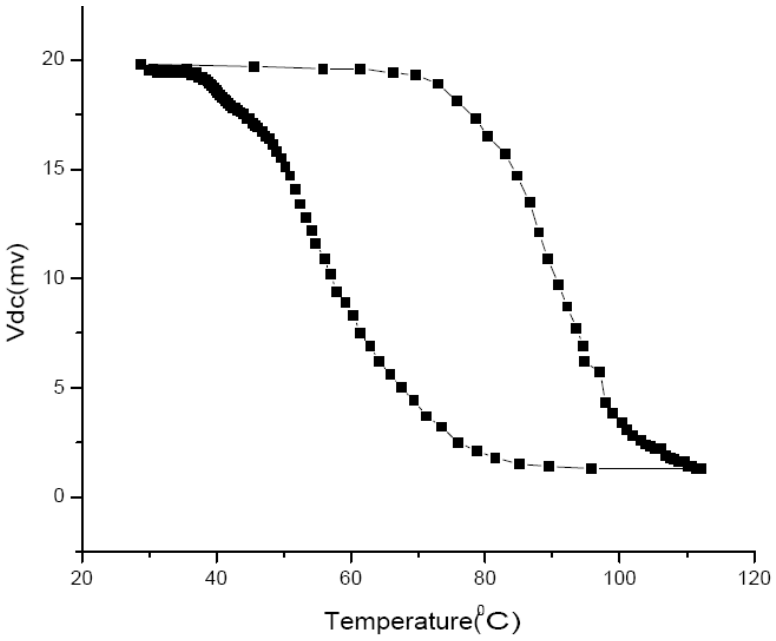

Figure 42 Vdc vs. Temperature of EVA770 (613Å) by OTM

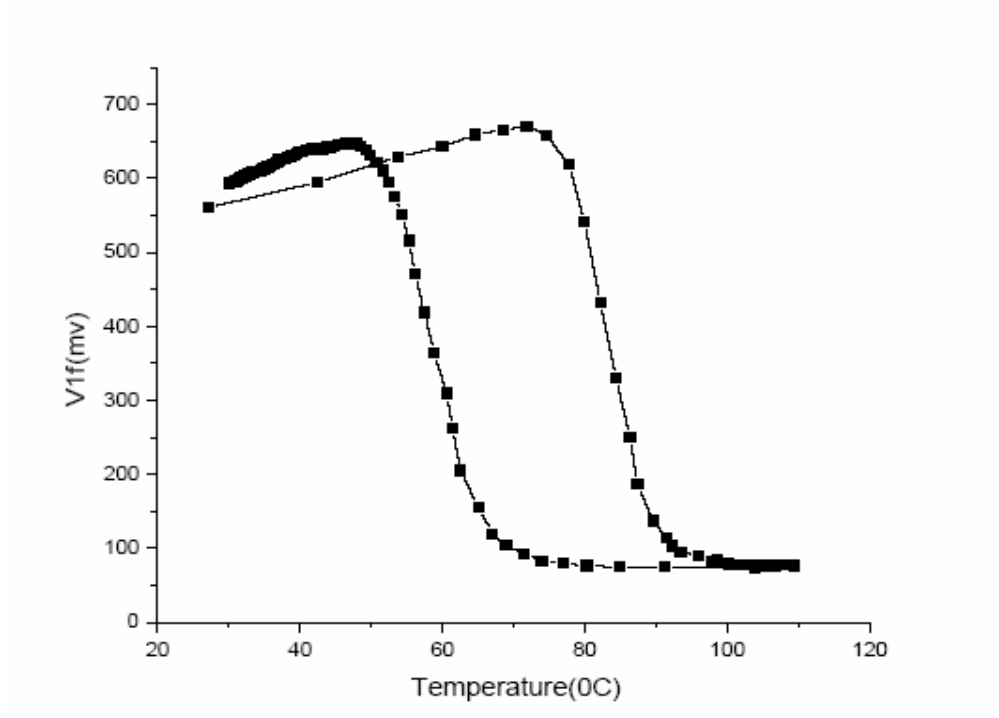

Figure 43 V1f vs. Temperature of EVA770 (785Å) by OTM

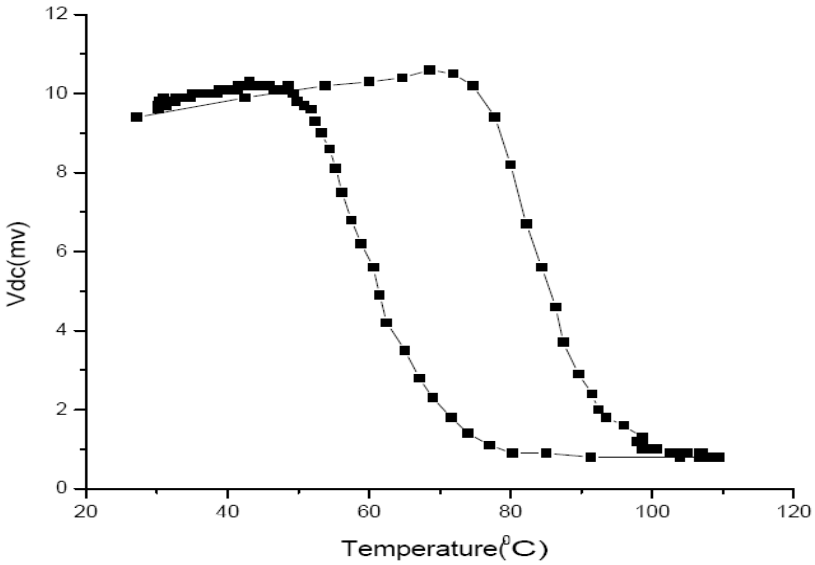

Figure 44 Vdc vs. Temperature of EVA770 (785Å) by OTM

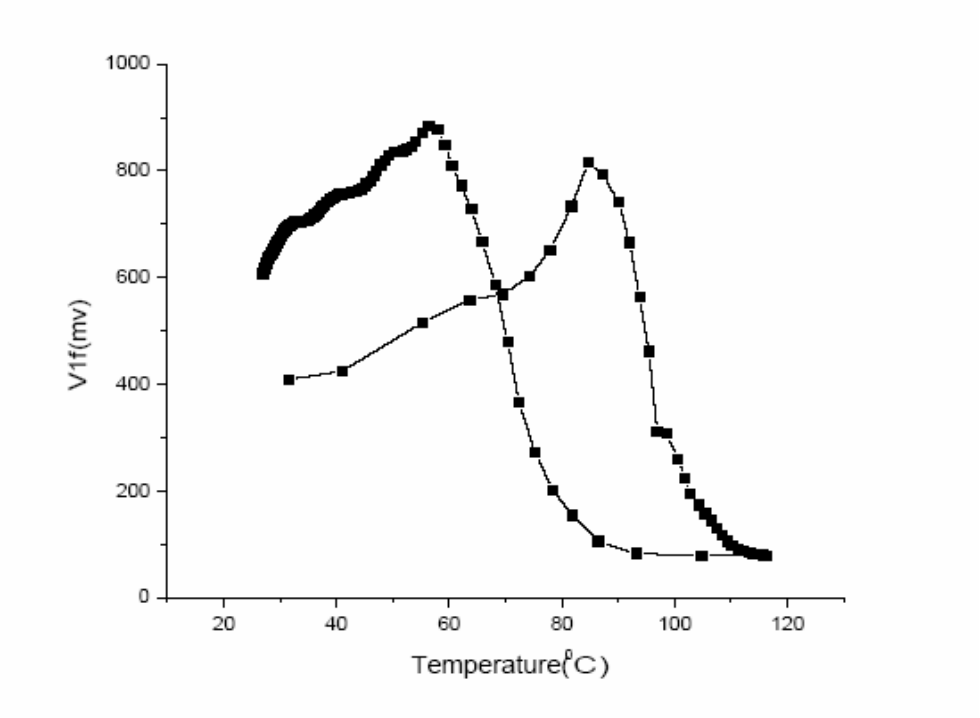

Figure 45 V1f vs. Temperature of EVA770 (1866Å) by OTM

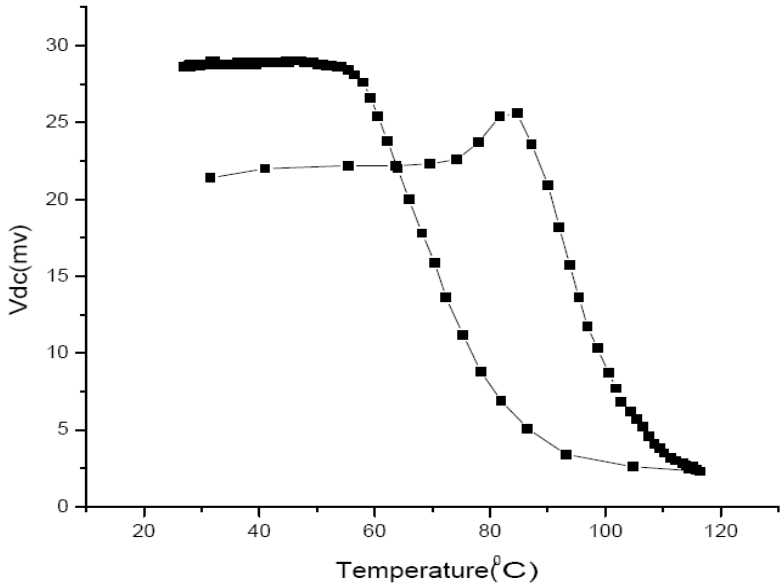

Figure 46 Vdc vs. Temperature of EVA770 (1866Å) by OTM

Thickness	116Å	262Å	352Å	431Å	613Å	785Å	1866Å
Melting Temperature	72^0C (345K)	78^0C (351K)	75.5^0C (348.5K)	86^0C (359K)	90^0C (363K)	87^0C (360K)	95^0C (368K)

Table 5 Melting Temperature vs. Film Thickness of EVA770 by OTM

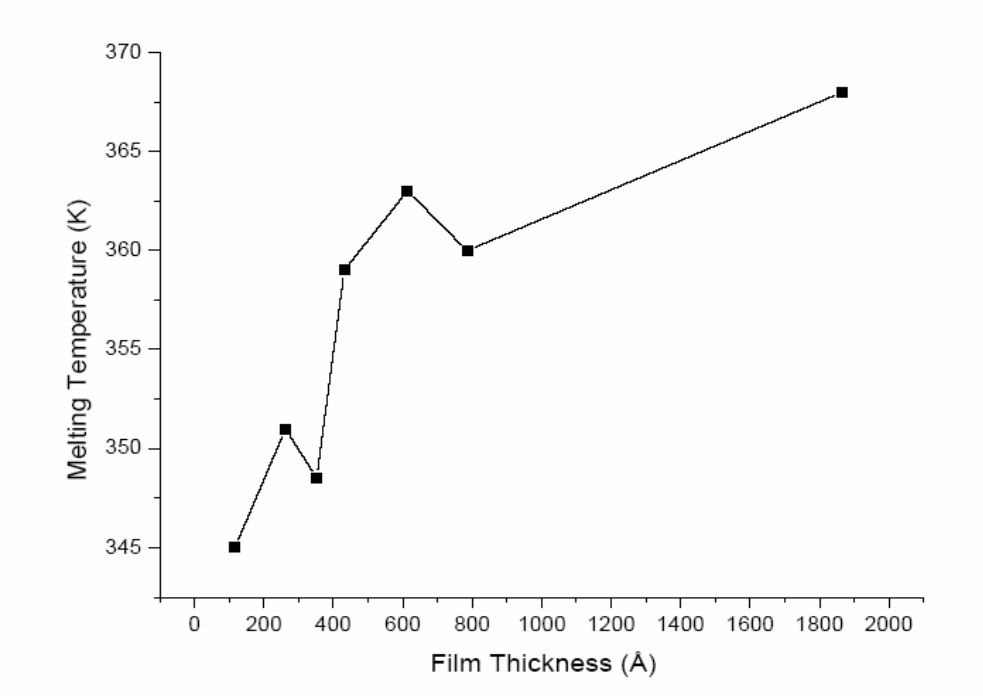

Figure 47 Melting Temperature vs. Film Thickness of EVA770 by OTM

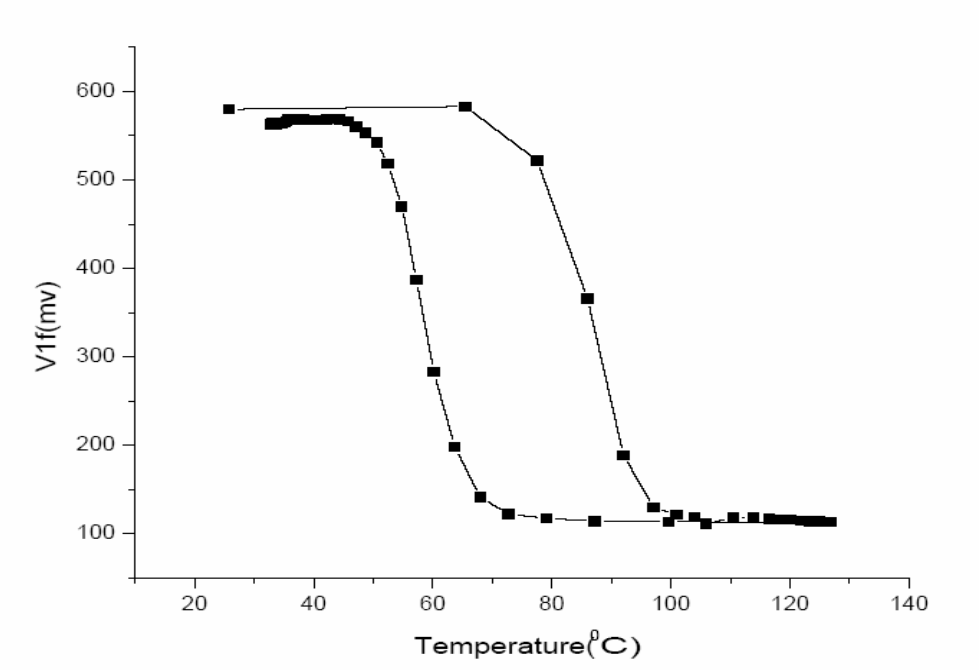

Figure 48 V1f vs. Temperature of LLPDE (182Å) by OTM

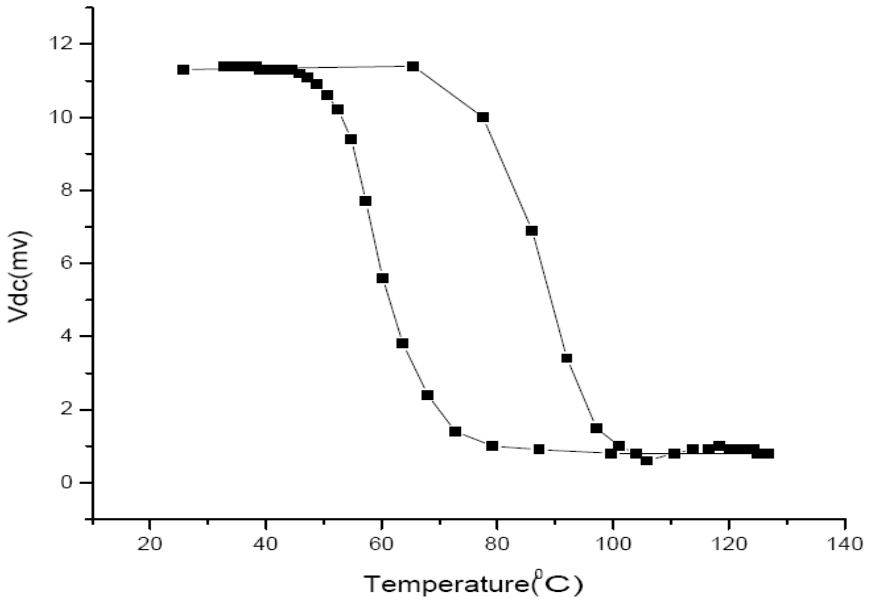

Figure 49 Vdc vs. Temperature of LLPDE (182Å) by OTM

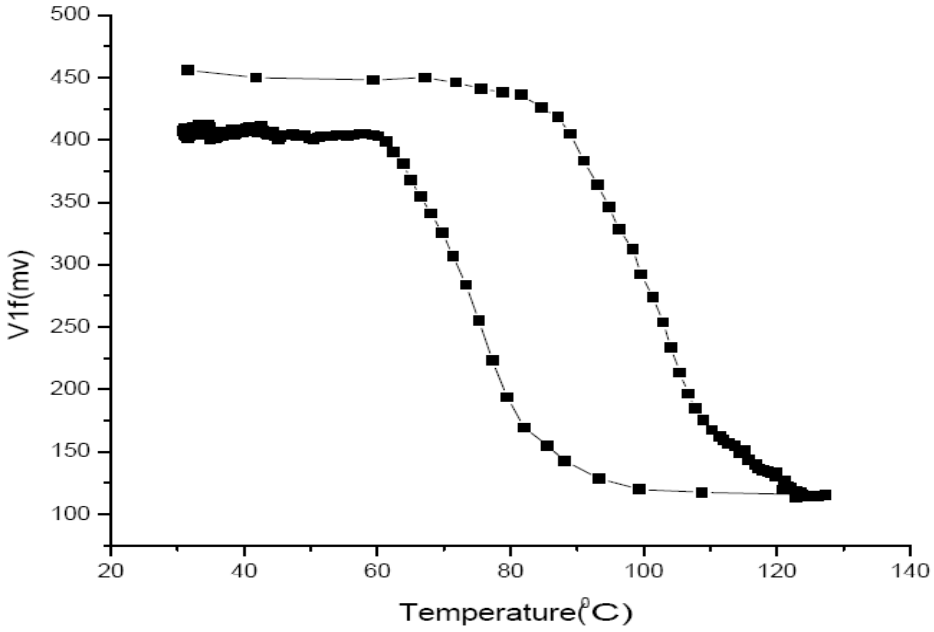

Figure 50 V1f vs. Temperature of LLPDE (230Å) by OTM

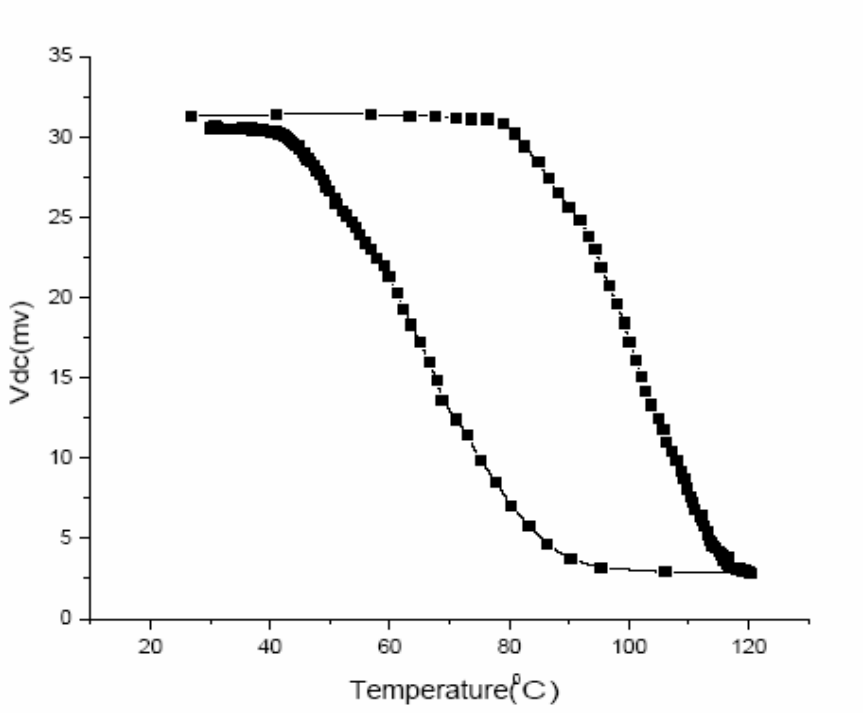

Figure 51 Vdc vs. Temperature of LLPDE (230Å) by OTM

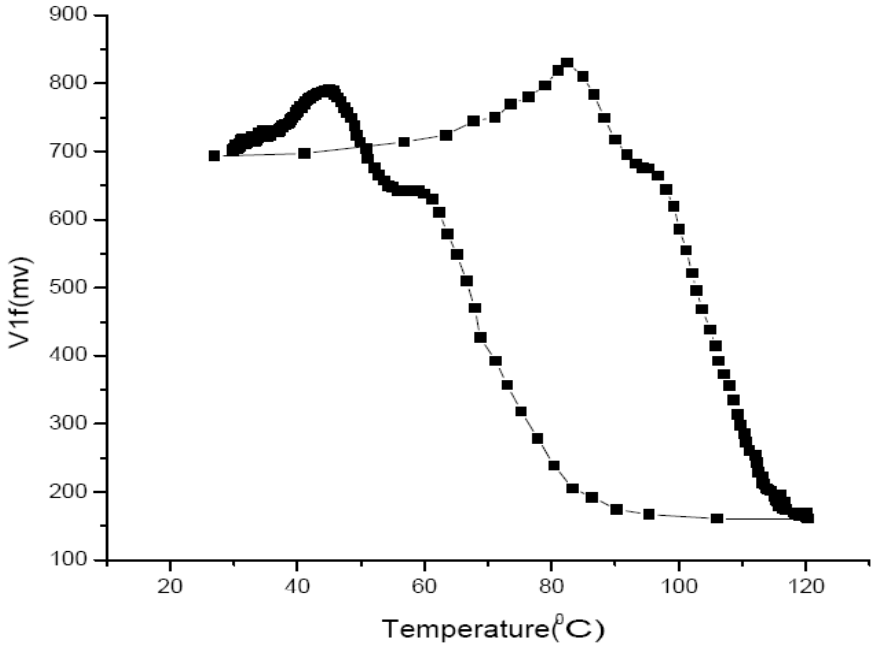

Figure 52 V1f vs. Temperature of LLPDE (241Å) by OTM

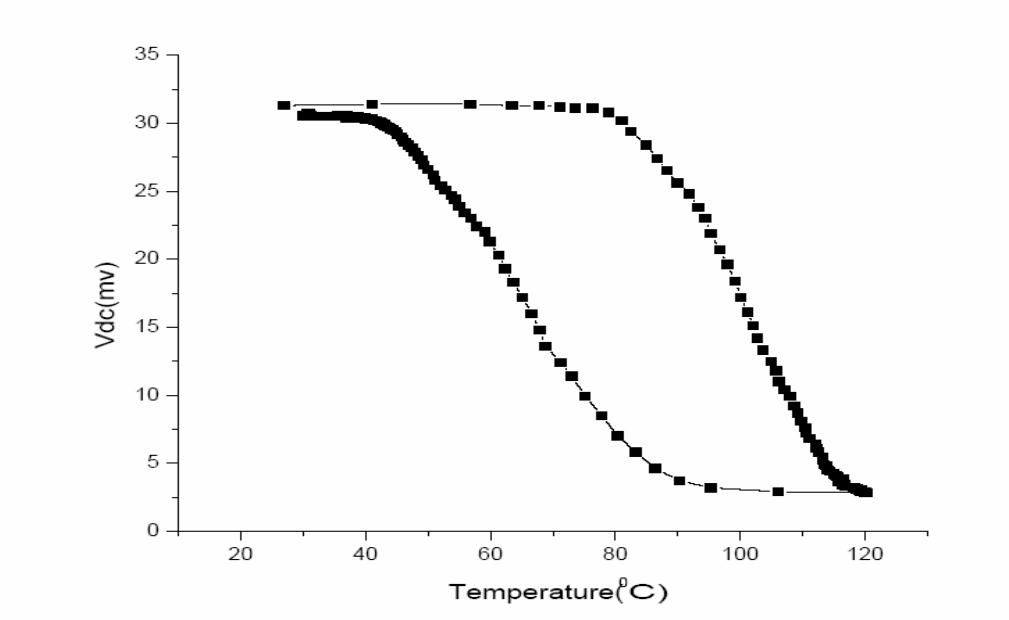

Figure 53 Vdc vs. Temperature of LLPDE (241Å) by OTM

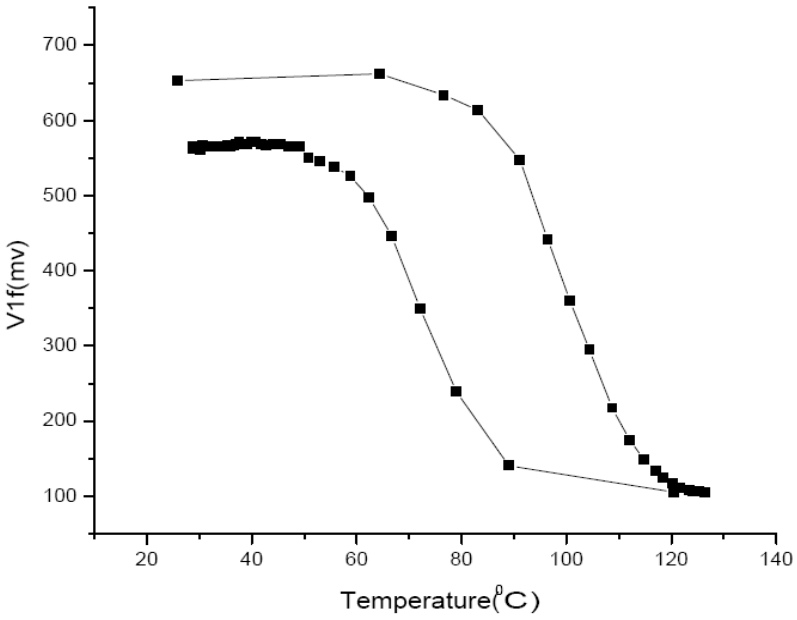

Figure 54 V1f vs. Temperature of LLPDE (420Å) by OTM

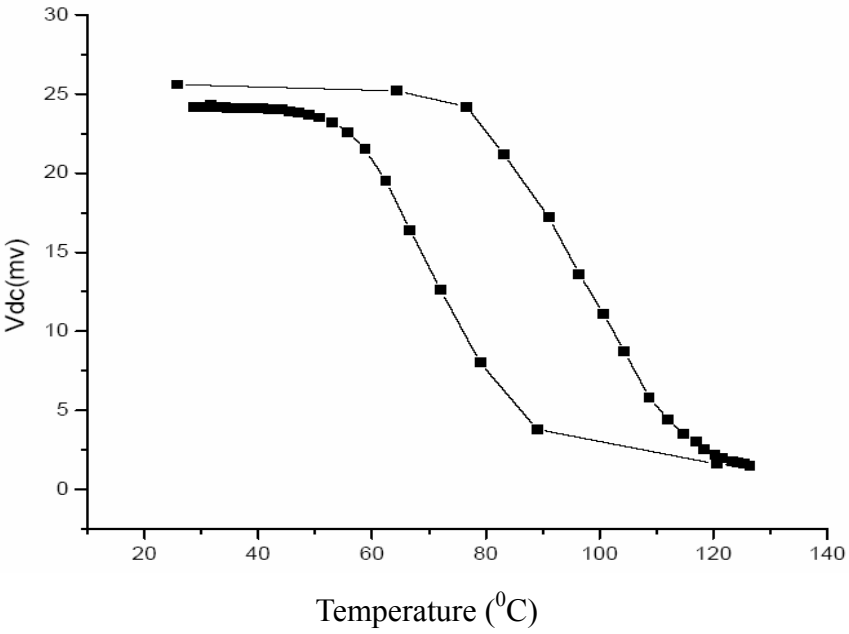

Figure 55 Vdc vs. Temperature of LLPDE (420Å) by OTM

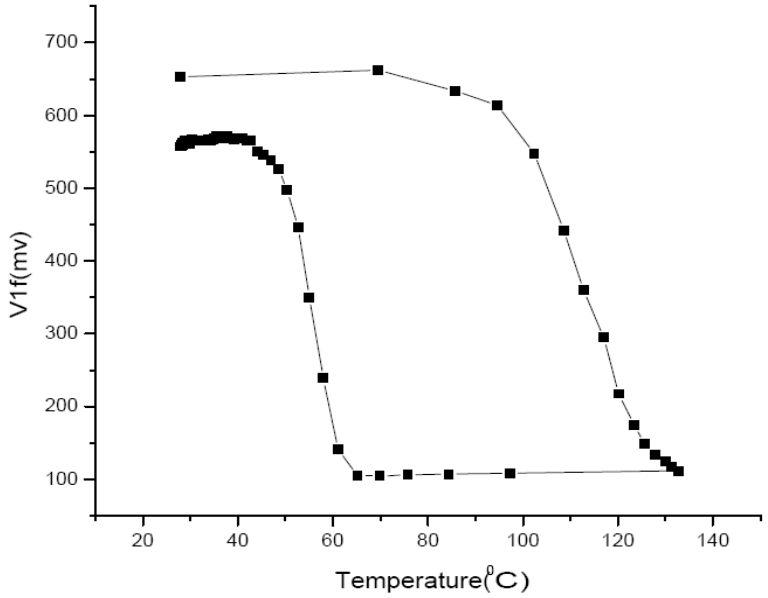

Figure 56 V1f vs. Temperature of LLPDE (846Å) by OTM

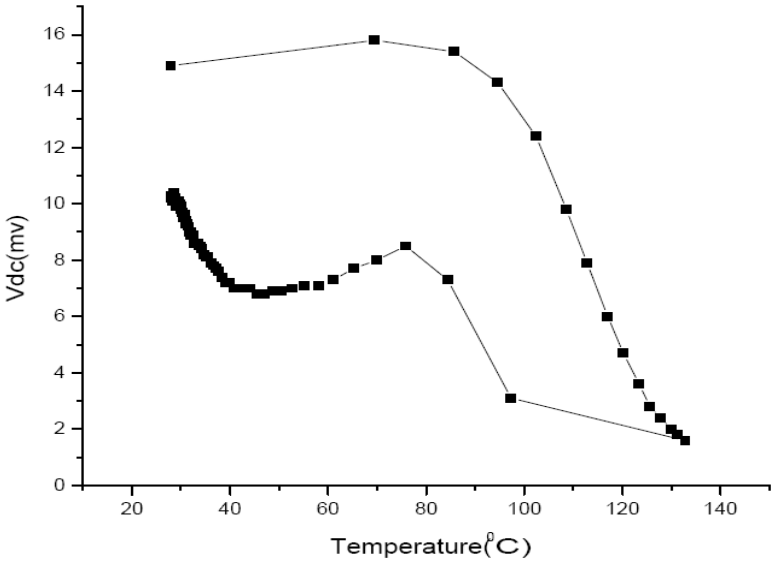

Figure 57 Vdc vs. Temperature of LLPDE (846Å) by OTM

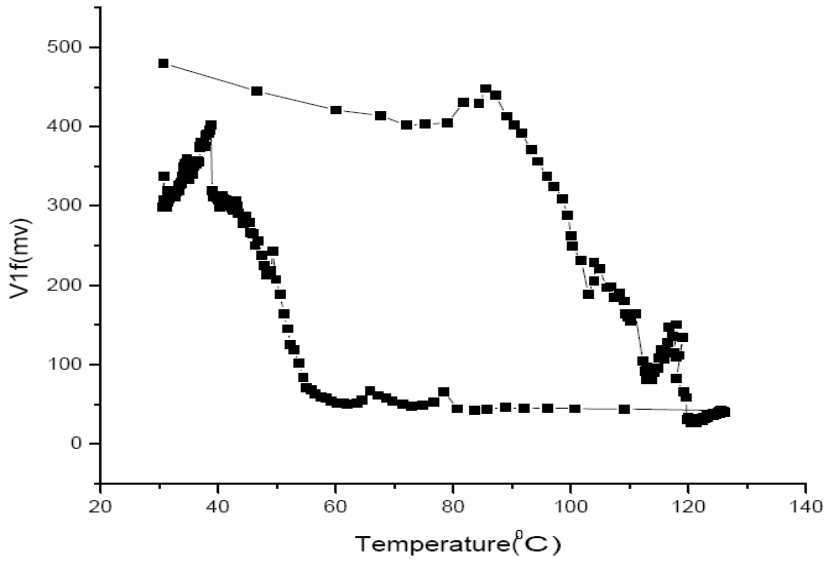

Figure 58 V1f vs. Temperature of LLPDE (1412Å) by OTM

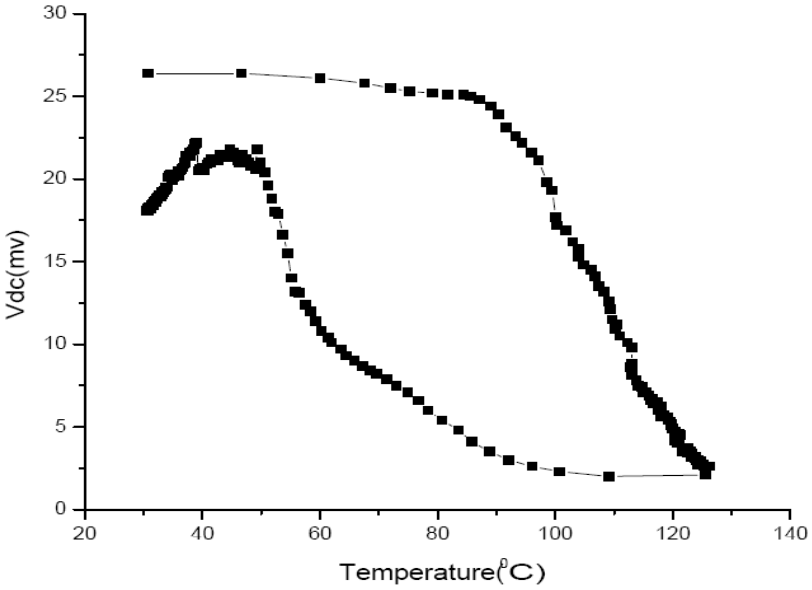

Figure 59 Vdc vs. Temperature of LLPDE (1412Å) by OTM

Thickness	182Å	230Å	241Å	420Å	846Å	1412Å
Melting Temperature	90^0C (363K)	95^0C (368K)	100^0C (373K)	105^0C (378K)	112^0C (385K)	110^0C (383K)

Table 6 Melting Temperature vs. Film Thickness of LLPDE by OTM

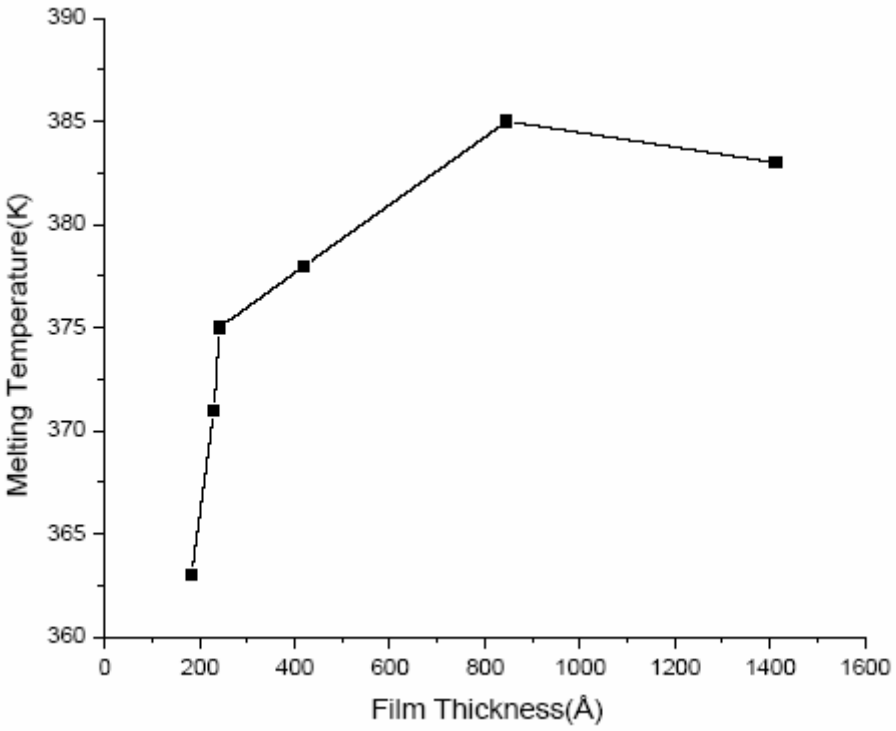

Figure 60 Melting Temperature vs. Film Thickness of LLPDE by OTM

Reference

1. D. Gupta, Paul S. Ho, Diffusion Phenomena in Thin Films and Micro-electronic Materials, Noyes Publications, NJ, (1998).
2. Scott Sills and Rene M. Overney, Interfacial Glass Transition Profiles in Ultra Thin Spin Cast Polymer Films, Journal of Chemical Physics, Volume 120 Number11 (March, 2004): p.5334-5337.
3. James R. Webster, Thin Film Polymer Dielectrics for High-Voltage Application under Severe Environment. Thesis for Master of Science Degree, Virginia Polytechnic Institute and State University (May, 1996).
4. S.J. Kwoun, R.M. Lec, B.Han and F.K.Ko, Polymer Nano-fiber Thin Films for Biosensor Applications, Proceedings of the IEEE 27th Annual Northeast Bioengineering Conference, 2001: p.9-10.
5. Detlef. M. Smilgies, Peter. Busch, Dorthe Posselt and Christine M. Paradalis, Characterization of Polymer Thin Films with Small Angle X-ray Scattering under Grazing Incidence (GISAXS), Synchrotron Radiation New, Issue 15.5 (2002).
6. P. Pissis, A. Kyritsis, G. Barut, R. Pelster and G. Nimtz, Grass Transition in 2- and 3- Dimensionally Confined Liquids, J. Non-Crystal Solids, Vol 235: p.444-449.
7. James N. Hay, the Physical Aging of Amorphous and Crystalline Polymer, Pure & Appl. Chem. V0l. 67, No. 11, 1995: p. 1855-1858.
8. Kilwon Cho and Fengkui Li, Reinforcement of Amorphous and Semicrystalline Polymer Interfaces via in-Situ Reactive Compatibilization, Macromolecules, Vol31,1998: p. 7495-9505.
9. Jacek Dudowecz, Karl F. Freed and Jack F. Douglas, The Glass Transition of Polymer Melts, J. Phys. Chem. B2005: p.21285-21292.
10. Materials Science and Engineering, Division of Engineering, The University of Edinburgh, Introduction to Polymers: p.1-13.

11. C.C. White, K. B. Migerler and W. L. Wu, Measuring Tg in Ultra-thin Polymer Films with an Excimer Fluorescence Technique, Polymer Engineering and Science, September 2001, Vol.41, N0.9: p.1497-1504.
12. H. Baur, Theoretical Aspects of Polymer Melting, Pure & Appl. Chem., Vol. 52: p.457-463.
13. Koji, Yamada, Masamichi Hikosaka, Akihiko Toda, Shinichi Yamazaki and Katsuharu Tagashira, Equilibrium Melting Temperature of Isotactic Polypropylene with High Tacticity, Macromolecules, 2003, 36: p. 4802-4812.
14. E. Donth, Dynamic or Configurational Approach to the Glass Transition, J. Non-Cryst. Solids, Vol.307, 2002: p.364-375.
15. J.A. Forrest, K. Dalnoki-Veress and J.R. Dutcher, Physical Review E, 56, 1997: p.5705.
16. Kim, J. H. Jang, J. and Zin, W. C. Macromol, Rapid Commun. 2001, 22: p.386.
17. Y. Wang, M. Rafailovich, J. Sokolov, D. Gersappe, T. Araki, Y. Zhou, A. D. L. Kilcoyne, H. Ade, G. Marom and A. Lustiger, Substrate Effect on the Melting Temperature of Thin Polyethylene Films, Physical Review Letters, January 2006: p.028303(1-4).
18. Cliver Li, Doctoral Dissertation, SUNY, Stony Brook University 2005: p.58-74.
19. Dupont™ Elvax®, Dupont Industrial Polymers, Elvax® Wires and Cable Product Guide.
20. J. Michl and E. W. Thulstrup, Spectroscopy with Polarized Light, VCH, c1995.
21. Masud Mansuripur, Classical Optics and Its Applications, Cambridge, UK , Cambridge University Press, 2002.
22. William A. Shurcliff, Polarized light: Production and Use, Cambridge, Harvard University Press (1962).
23. D. Clarke, J. F. Grainger, Polarized Light and Optical Measurement, 1971.
24. Dennis H. Goldstein, Polarization Analysis and Measurement, San Diego, Claifornia 1967.
25. Collett and Edward, Polarized Light : Fundamentals and Applications, 1993.

26. David S. Kliger, James W. Lewis and Cora Einterz Randall, Polarized Light in Optics and Spectroscopy, Boston: Academic Press, 1990.
27. Craig Frederick Bohren and Eugene Edmund Clothiaux, Fundamentals of Atmospheric Radiation, Applied Optics, Vol. 33: p. 4754–4755.
28. Kwan, A., Dudley, J., and Lantz, E, Who Really Discovered Snell's Law, Physics World April 2002, Institute of Physics Publishing, Bristol and Philadelphia.
29. Bruce Hapke, Theory of Reflectance and Emittance Spectroscopy, Cambridge [England]: Cambridge University Press, 1993.
30. J.C. Kemp, Polarized Light and Its Interaction with Modulating Devices, Hinds International Inc. 2002.
31. A. D L. Humphris, M. J. Miles, J. K. Hobbs, A Mechanical Microscope: High-Speed Mtomic Force Microscopy, Applied Physics Letters 86, 034106 (2005).
32. H. Marand, Class Notes Physical Chemistry of Polymers, Virginia Tech, 1998.
33. Srinivas, S. Marand, On the Applicability of the Linear Hoffman-Weeks Extrapolation to Determine the Equilibrium Melting Temperature of Semi-rigid Polymer, American Physical Society, Annual March Meeting, March 17-21, 1997.